KERNFORSCHUNGSZENTRUM

KARLSRUHE

April 1970

KFK 1172

Institut für Experimentelle Kernphysik

The Final State Interaction in the Reaction p+d ⇒ p+p+n

H. Brückmann, W. Kluge, H. Matthäy, L. Schänzler, K. Wick

GESELLSCHAFT FUR KERNFORSCHUNG M. B. H.

KARLSRUHE

KERNFORSCHUNGSZENTRUM KARLSRUHE

April 1970 KFK 1172

Institut für Experimentelle Kernphysik

The final state interaction in the reaction p+d → p+p+n

H. Brückmann, W. Kluge, H. Matthäy, L. Schänzler

K. Wick

Gesellschaft für Kernforschung m.b.H Karlsruhe

Abstract

The three-particle reaction d+p → p+p+n has been investigated systematically at a deuteron bombarding energy of 52 MeV. Kinematically complete coincidence experiments have been carried out. Either two of the protons or the neutron and a proton were detected in coincidence. The kinematical conditions were chosen to observe the effects of n-p and p-p final state interaction predominantly. The Watson-Migdal model of final state interaction was used to analyse the data.

An angular distribution was obtained for the production of singlet and triplet final state interacting n-p pairs with zero relative energy in the n-p subsystem. A quantitative relation is established connecting the angular distribution of elastic p-d scattering with the measured angular distribution for triplet final state interaction in the three-nucleon reaction.

The validity of the two-step reaction model of n-p final state interaction was checked by angular correlation measurements where one detector was kept at a fixed position. The applicability of the model is confirmed by the experimental results.

The p-p final state interaction was investigated at identical kinematical conditions. The angular distribution in the p-p subsystem turns out to be slightly anisotropic but the production of p-p pairs in the ^1S_o state is dominating.

The result of the systematic study of the reaction p+d → p+p+n proves that values of the n-p and p-p scattering length can be extracted with a high degree of reliability from three-particle reactions at properly chosen kinematical conditions.

1. Introduction

In the past in nuclear physics considerable effort has been concentrated on the experimental and theoretical investigation of few body problems. Within this field particular interest is paid to the study of the simplest nuclear reactions p+d → p+p+n and n+d → p+n+n involving three nucleons only. There are two main relevant questions to be answered by a systematic investigation of these two reactions.

Firstly one aims at a complete understanding of the reaction mechanism responsible for such a three nucleon break-up. Therefore one is interested in the limits of applicability of special reactions models.

Secondly one wants to determine the way to extract properties of the two-nucleon interaction from a three-particle reaction. The answer to this question is particularely needed for the determination of neutron-neutron scattering parameters. At laboratory conditions the n-n interaction can be studied only in three particle reactions like n+d → p+n+n [4b]. Prior to the extraction of reliable n-n scattering parameters the limits of applicability of the final state interaction model have to be determined by comparing n-p final state interaction data with the parameters of free neutron-proton scattering. From the experimental point of view such a comparison can be carried out more conveniently by the investigation of the reaction p+d → p+p+n.

A complete theoretical description of a three particle reaction has to be based on calculations which solve the many body problem by using only the knowledge of the nucleon-nucleon forces. From the point of view of a formal scattering theory the three body problem is to be regarded as principally solved (see e.g. Ref. [1] and [2]).Numerical calculations however require such extremely large computer capacities that approximations have to be used and only a few authors have presented numerical results which can be compared directly with experimental data (see e.g. Ref. [2]).

The experimental data available in the literature for the reaction p+d → p+p+n contain to a considerable extent results on single counter experiments where only one of the outgoing particles was detected (kinematically incomplete experiments, see e.g. Ref.[3]).Only a small number of groups reported on coincidence experiments which are kinematically complete [4,5,6]. Almost none of the experiments published up to now covered the effects of final state interaction systematically in a very broad kinematical region. This is partly due to the fact that mostly protons have been used as projectiles and in this case the quasielastic scattering process can be observed more conveniently.

We have studied the reaction p+d → p+p+n induced with 52 MeV deuterons by means of coincidence experiments in a wide region of kinematics. The aims of our experiments were:

a) to measure an angular distribution for the production of final state interacting neutron-proton singlet and triplet pairs;

b) to check the applicability of the Watson-Migdal model [7] of final state interaction (FSI) at many different kinematical conditions;

c) to check the validity of the two-step reaction model by measuring the angular distribution in the neutron-proton center-of-mass subsystem;

d) to investigate the proton-proton FSI down to very low relative energies where free p-p scattering cannot be studied experimentally;

e) to compare the neutron-proton FSI with the proton-proton FSI at kinematical identical conditions;

2. Experimental procedure

The focussed beam of 52.3 MeV deuterons from the Karlsruhe isochronous cyclotron was used to bombard a polyethylene target. The set-up is shown schematically in Fig. 1. Two detectors placed at angles θ_3 and θ_4 were used to detect either the two protons or one of the protons and the neutron in coincidence. A plastic scintillator was used to detect the neutrons whereas the protons were detected by NaI(Tl) scintillators. Distances between target and detectors of up to 120 cm allowed an excellent angular resolution of 0.3 - 0.5° typically. Such large distances were also necessary for the measurement of the neutron energy by time-of-flight technique and allowed the particle identification to be made by time-of-flight technique [8]. An energy signal E and a timing signal τ is derived from each detector. The timing signals τ and reference pulses from the cyclotron RF are fed to special electronic circuits which deliver two time-of-flight signals. The detailed features of this electronic system are described in [8]. The two energy signals and the two time-of-flight signals are fed via a data acquisition system (DATA) [9] on-line to a CDC 3100 computer. In this way the total information of each coincidence event is assembled in one or two 24 bit computer words and recorded on magnetic tape. The final data processing was carried out with an IBM 360/65 computer. The details of the experimental set-up and the electronic data processing are described elsewhere [5,9].

The total charge of the incident beam was measured with a Faraday cup and a current integrator. An additional monitor detector was placed at a fixed angle to be independent from changes in the target thickness with time and from errors in the charge measurement. The spectrum of the monitor was registered separately.

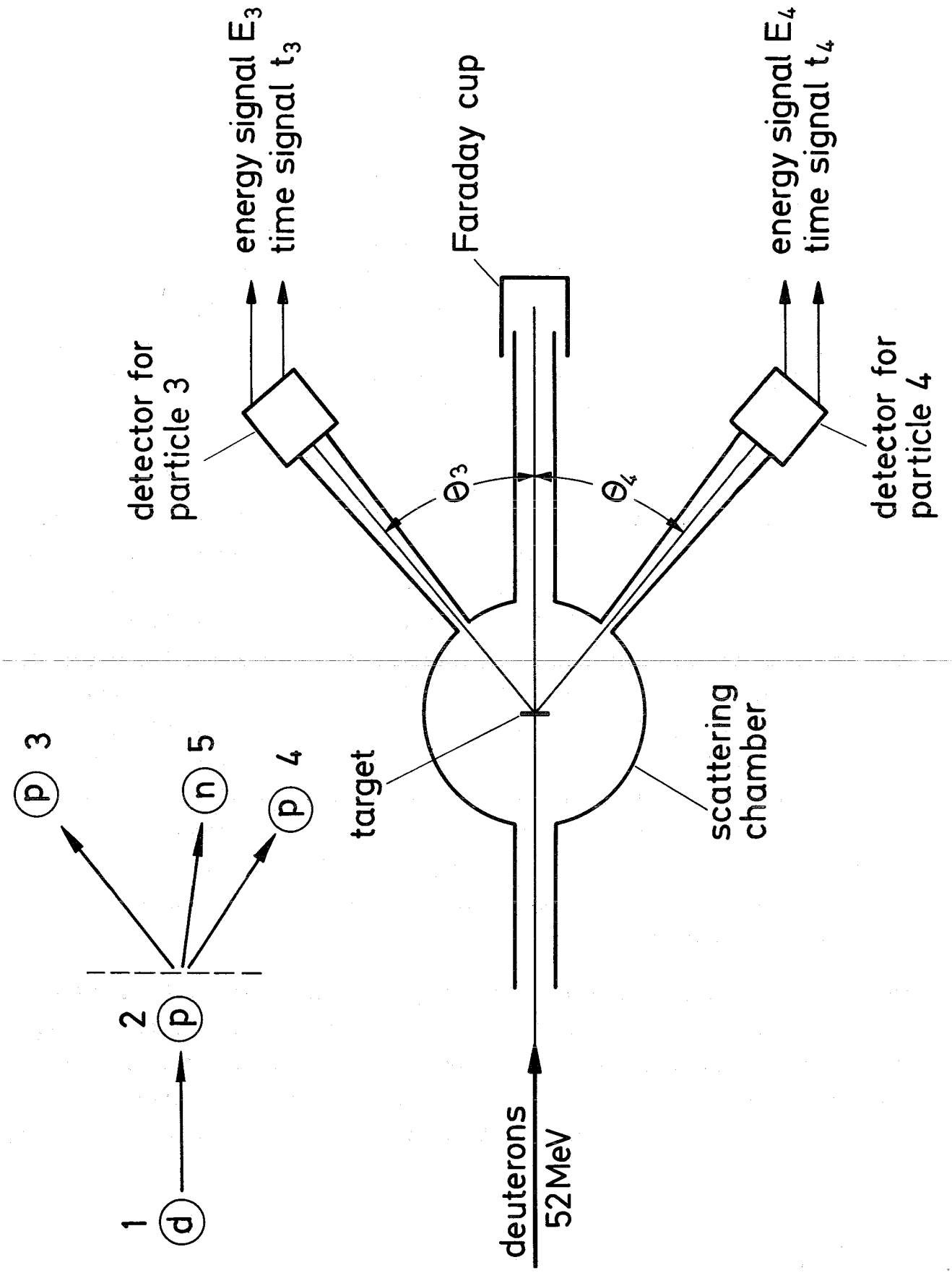

Fig. 1 The experimental set up and the nomenclature used for the particles and angles.

3. The neutron-proton final-state interaction in the reaction p+d → p+p+n

3.1 An experimental example and the methods of analysis

The n-p final-state interaction was investigated in the reaction

p+d → p+p+n

(denoted in the following as particles 1+2 → 3+4+5)

by observation of coincidences between the two outgoing protons. The protons have the energies E_3 and E_4. At two fixed angles θ_3 and θ_4 the energies of these two protons are correlated by the kinematics and all the coincidence events are located on a kinematically allowed curve in the E_3-E_4 plane. [5,10].

In general several different reaction mechanisms are contributing in a rather complex way to the three-particle cross-section. An advantage of kinematically complete experiments is that a proper choice of the pair of angles allows the reaction to be observed at kinematical conditions where one reaction mechanism is dominating. For instance at small relative energies E_{np} (e.g. E_{35} or E_{45}) one expects the n-p final-state interaction to be dominant. Therefore one wants E_{np} to reach down to zero along the kinematically allowed curve. This condition fixes θ_4 after θ_3 is chosen or vice versa [5]. Fig. 2a shows as an example the kinematically allowed curve for the set of angles θ_3=42.0° and θ_4=25.3°. At fixed angles θ_3 and θ_4 the relative energy E_{45} is a single valued function of the energy E_3. A corresponding relation holds also for E_{35} and E_4 [5,10]. The energies E_{45} or E_{35} have their minimum values at the points where E_3 or E_4 respectively have their maximum. This special feature of the kinematics leads to a very slow variation of the relative energies in the neighbourhood of these extrema. The phenomena is called the kinematical lupe effect of three particles reactions and can be observed in kinematically complete experiments only. The main contribution of the FSI between the proton 3 and the neutron 5 will appear in the region labelled in Fig.2a as FSI(3,5). The n-p FSI of the

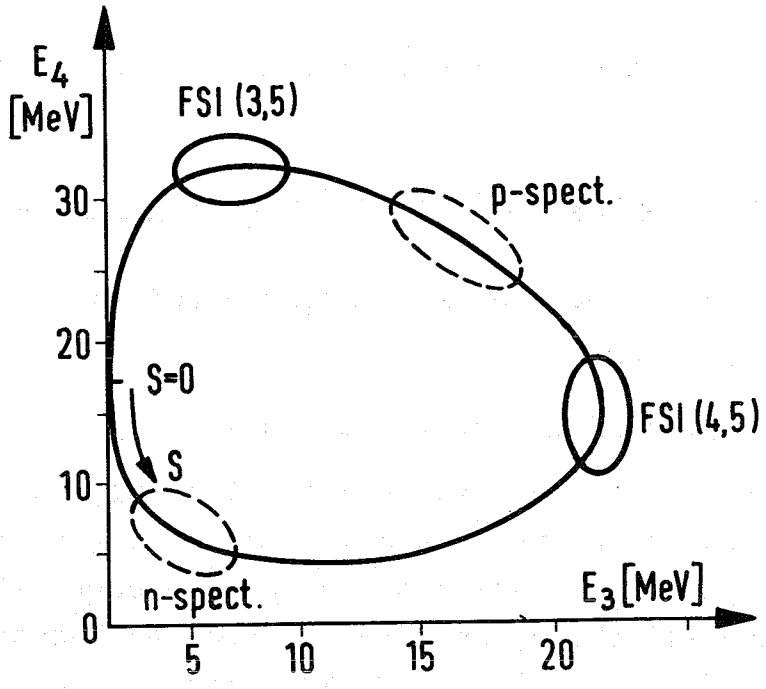

Fig. 2a)

The kinematically allowed curve in the E_3-E_4 plane. Regions where final-state interaction is expected are denoted by FSI. In quasi-elastic scattering a proton might be the spectator particle (p-spect.) or the neutron does not participate in the reaction (n-spect.). S is the arc length along the kinematical curve (see eq. 1)

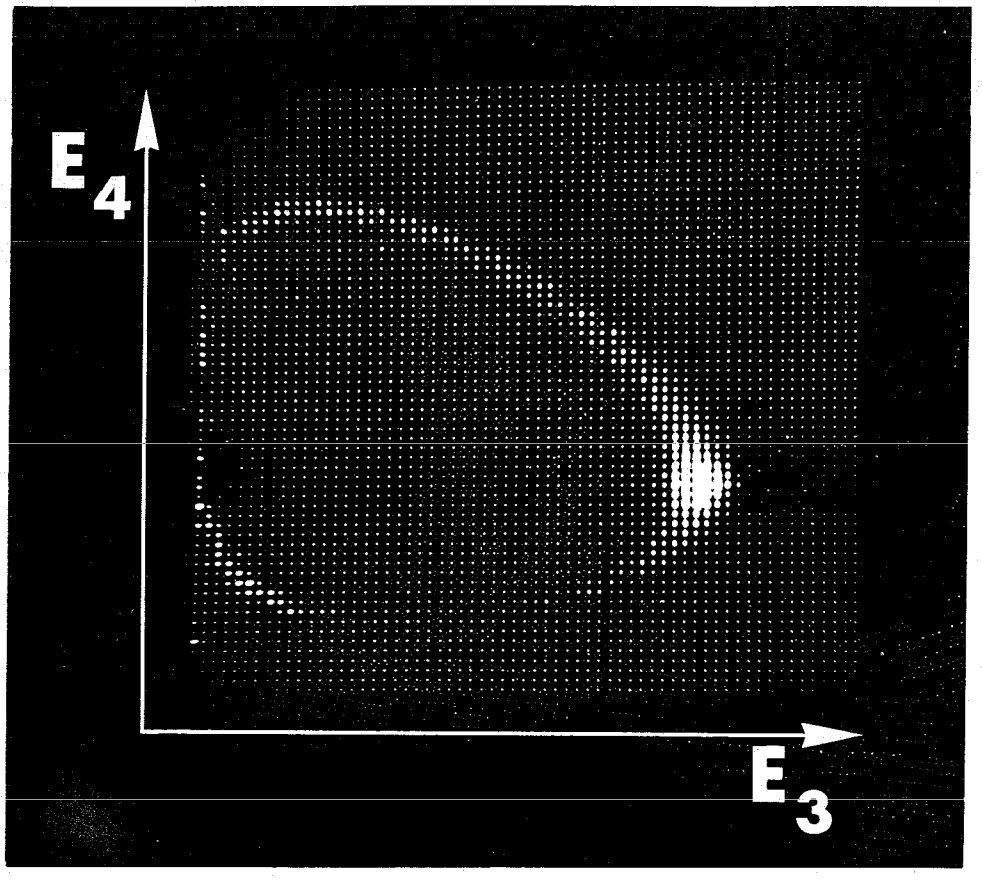

Fig. 2b)

The corresponding experimental data shown as a map display in an array of 64×64 channels.

(4,5)-pair will be observed predominantly in the region FSI(4,5). In the example of Fig. 2a only the energy E_{45} becomes zero and thus a particular large FSI contribution is expected at FSI(4,5). The minimum for the energy E_{35} is 1,15 MeV and only a very small FSI contribution is expected from the singlet state interaction of the particles 3 and 5.*

In a quasielastic scattering [11,4b] either the neutron or the proton of the projectile deuteron can act as a spectator particle. If the neutron is taken to be the spectator the main contribution of the spectator effect will be observed in the region labelled as "n-spect". If the proton however acts as a spectator an enhancement of events will be found in the region denoted by "p-spect". In the example of Fig. 2a a proton spectator has to carry off a rather high momentum from the internal momentum distribution in the deuteron and hence the effect of quasielastic scattering can be neglected. At these kinematical conditions one expects the investigation of the n-p FSI between the particles 4 and 5 to be possible with only negligible distortions from other reaction mechanisms.

The corresponding experimental data are shown in the map display of Fig. 2b in an array of 64 × 64 channels. The experimental arrangement in use allows us to register even such coincidence events where one particle has a very low energy. As is seen from the map display the coincidence events populate the whole kinematical curve. The FSI enhances the cross-section strongly at high values of the energy E_3 and a FSI peak is clearly visible. Random coincidences have been subtracted as discussed in [9]. For the analysis of the data the number of coincidence events is projected onto the kinematical curve of Fig. 2a. The position on the kinematical curve is characterized by the arc length S defined by [10]

---

* The contribution of triplet FSI in the n-p pair (3,5) is negligible because the particular pair of angles corresponds to the minimum in the angular distribution of triplet FSI (see Fig. 7).

$$S = \int \sqrt{(dE_3)^2 + (dE_4)^2} \qquad (1)$$

Fig. 3 shows the experimentally obtained three-particle cross-section plotted versus the arc length S and the proton energy E_3. The distribution of events along S contains the physical information on the three-particle reaction. In the following a brief description of the methods of analysis will be given.

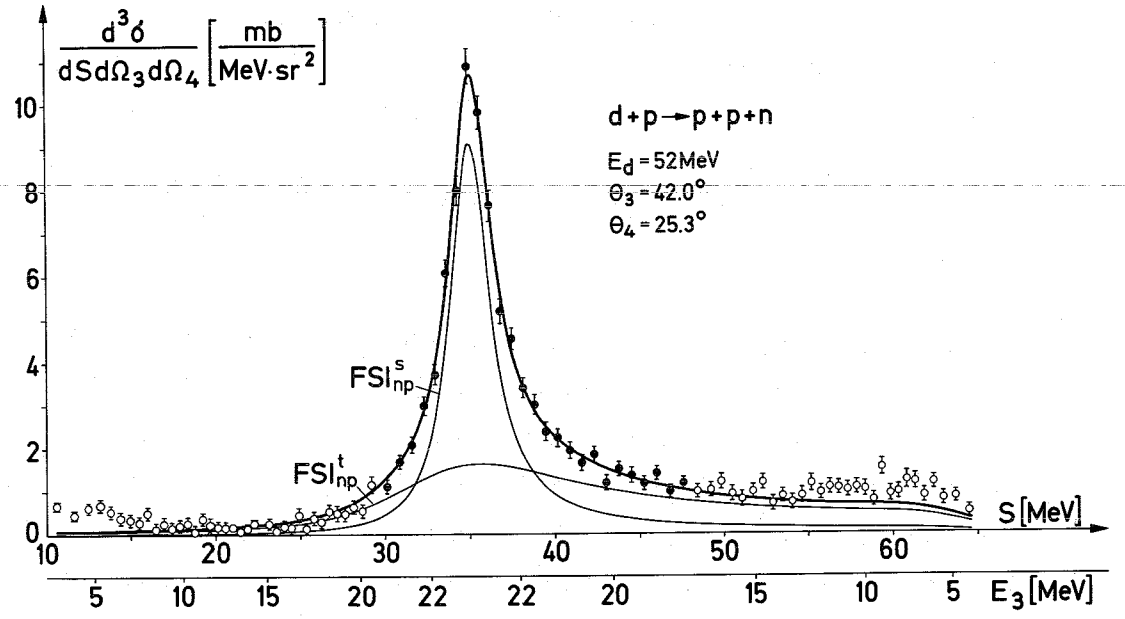

Fig. 3

The three particle cross-section of the reaction d+p → p+p+n plotted versus the arc length S and the proton energy E_3. The solid curve is the result of an analysis based on formula 5 assuming an incoherent superposition of FSI in singlet state (FSI^s_{np}) with FSI in triplet state (FSI^t_{np}).

The three-particle cross-section is given by

$$\frac{d^3\sigma}{dS d\Omega_3 d\Omega_4} = \frac{2\pi}{\hbar} \cdot \frac{m_1}{p_1} |T_{fi}|^2 \cdot \rho_S (E_3, E_4) \qquad (2)$$

where T_{fi} is the three-particle transition matrixelement, ρ_S is the phase space factor [10], m_1 and p_1 are the mass and the momentum of the projectile deuteron. Describing the n-p FSI as a two-step reaction mechanism the matrixelement T_{fi} can be written according to Goldberger-Watson [12] as

$$\left[T_{fi}\right]^2 = F_{np}(E_{np}) \left[T^o_{fi}\right]^2 \qquad (3)$$

F_{np} is the enhancement factor for the n-p FSI and $\left[T^o_{fi}\right]^2$ is the matrixelement for the production of the final state interacting n-p pair. Following the Watson model T^o_{fi} should depend only very weakly on the relative energy E_{np} and hence its variation with E_{np} is neglected in the analysis. The n-p pair can be produced in the singlet or the triplet state. Therefore two enhancement factors F^s_{np} and F^t_{np} have to be used [13].

Both factors are written in the following form

$$F_{np} = \frac{(\kappa^2+\alpha^2)^2 \cdot \frac{r_o^2}{4}}{(-\frac{1}{a} + \frac{r_o}{2}\kappa^2)^2+\kappa^2}$$

with

$$\alpha = \frac{1}{r_o}\left(1+\sqrt{1-\frac{2r_o}{a}}\right)$$

where $\kappa = (M \cdot E_{np}/\hbar^2)^{\frac{1}{2}}$ is the momentum of the neutron and the proton in the center-of-mass of the n-p pair, M is the mass of a nucleon, a is the scattering length, r_o the effective range and α is a

function of a and r_o as given in [12]. For only one n-p pair (with indices 4 and 5) interacting in the final state the incoherent superposition of the production of singlet and triplet states of the n-p pairs leads to the cross section

$$\frac{d^3\sigma}{dS\ d\Omega_3\ d\Omega_4} = \left[X^s_{np}(\theta_3)F^s_{np}(E_{45})+X^t_{np}(\theta_3)F^t_{np}(E_{45})\right]\cdot\rho_S(E_3, E_4) \qquad (5)$$

where e.g. $X^s_{np}(\theta_3)$ is given by

$$X^s_{np}(\theta_3) = \frac{2\pi}{\hbar}\cdot\frac{m_1}{p_1}\left|T^o_{fi}\right|^2_{\text{singlet}} \qquad (6)$$

X^s_{np} and X^t_{np} are factors which are proportional to the production probability of the n-p subsystem in the singlet and triplet states.

The expression (5) is used to determine the three parameters a^s, X^s_{np}, X^t_{np} by least-square-fit calculations. (For the least square-fit-only the data shown as full dots in Fig. 3 are used where the FSI(4,5) dominates). The analysis is insensitive to a variation of the parameters a^t, r^s, r^t. For these parameters the values known from free n-p scattering were therefore inserted:

$$a^t = (5.41 \pm 0.01)\ \text{fm}$$
$$r^s = (2.67 \pm 0.02)\ \text{fm}$$
$$r^t = (1.75 \pm 0.015)\text{fm}$$

The curves in the example of Fig. 3 represent the result of the least square fit calculations including the effects of angular resolution and the finite target thickness. It is obviously seen that the experimental data can excellently be fitted by expression (5) along the whole kinematical curve. Small differences arise only at very low and very high values of the arc length S.

As pointed out above one expects contributions of other reaction mechanisms in these regions. But in the example discussed here these contributions are seen to be negligible, at least in the region of dominating FSI. Hence this example is an appropriate one to determine a reliable value of the singlet scattering length a^s if the Watson formula holds. The result obtained is $a^s_{np} = -23.2$ fm which has to be compared with the value known from free n-p scattering $a^s_{free} = -(23.68 \pm 0.03)$ fm [14]. The result of the discussed example shows that the Watson-Migdal theory is very adequate to describe the cross-section as long as one chooses kinematical conditions where the contributions from other competing reaction mechanisms are kept at a minimum.

3.2. The angular distribution of the reaction p(d,d*)p

3.2.1 Experimental results

Coincidence experiments of the kind as illustrated in the proceeding section have been carried out at ten different pairs of angles. The aim was to measure angular distributions for the production of the n-p subsystem (d^*) in the singlet and the triplet states. As is pointed out in section 3.1 the d^* production cross-section is expected to have a maximum at a relative energy $E_{np} = 0$. Hence all pairs of angles were chosen in such a way that the corresponding kinematical curve contains at least one point where E_{np} is zero.

Fig. 4a-d shows some of the map displays and the corresponding coincidence spectra. The spectra are presented as a function of the arc length S and the proton energy E_3. Fig. 4a verifies the unique situation where n-p pairs with zero relative energy can be observed at two different points of the kinematical curve. The angles for this unique situation are $\theta_3 = \theta_4 = 27.7^\circ$. The single neutron can form a zero energy n-p system with each of the two protons. Two identical FSI peaks arise from these two n-p pairs. The pairs are denoted as (3,5) and (4,5) couples.

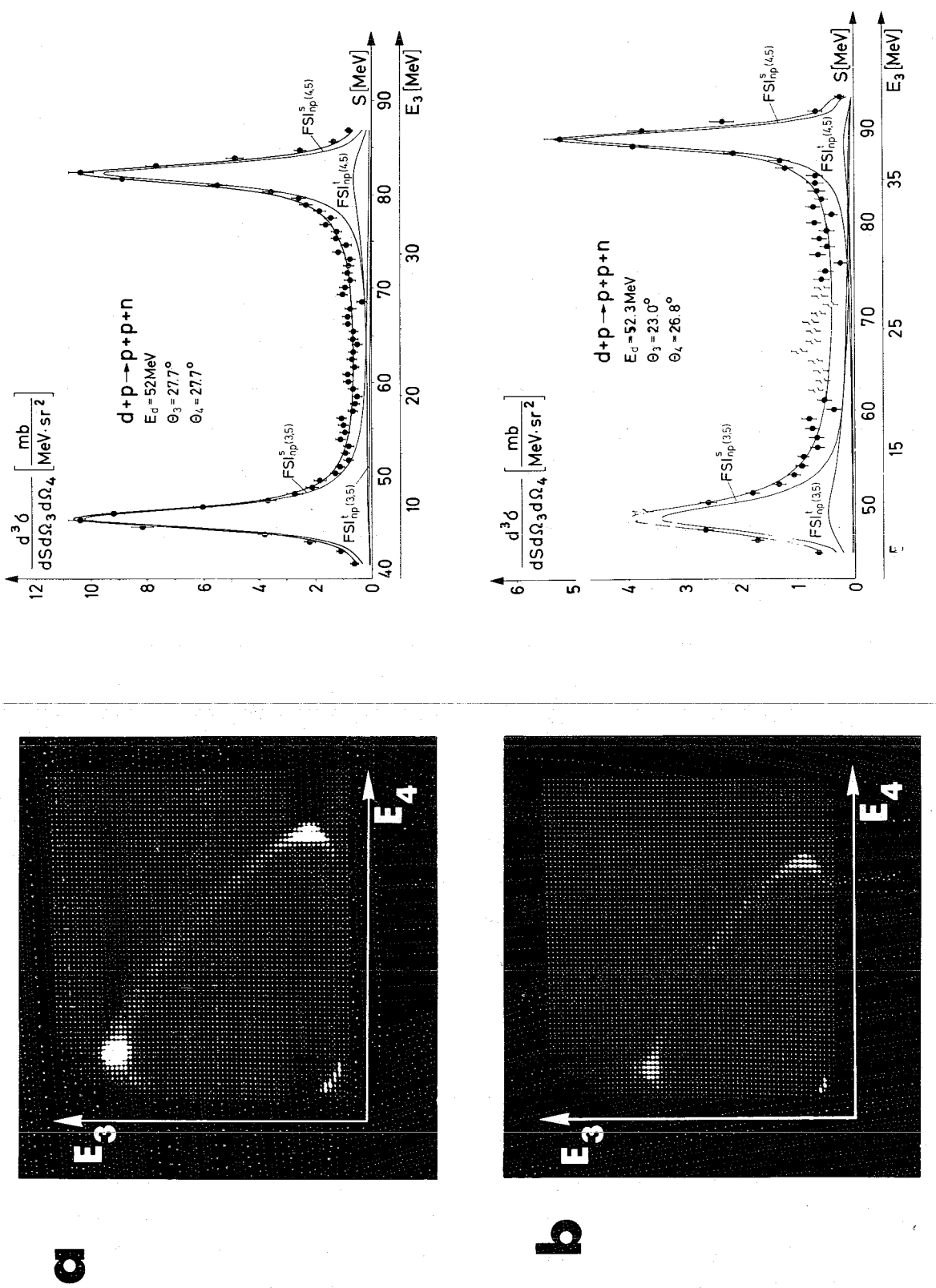

Fig. 4a)

The map display and the corresponding coincidence spectrum for the unique situation where two identical FSI-peaks arise. $\theta_3=\theta_4=27.7^\circ$. The denotation is the same as in Fig. 3.

Fig. 4b)

Experimental data for the set of angles $\theta_3=23.0^\circ$ and $\theta_4=26.8^\circ$.

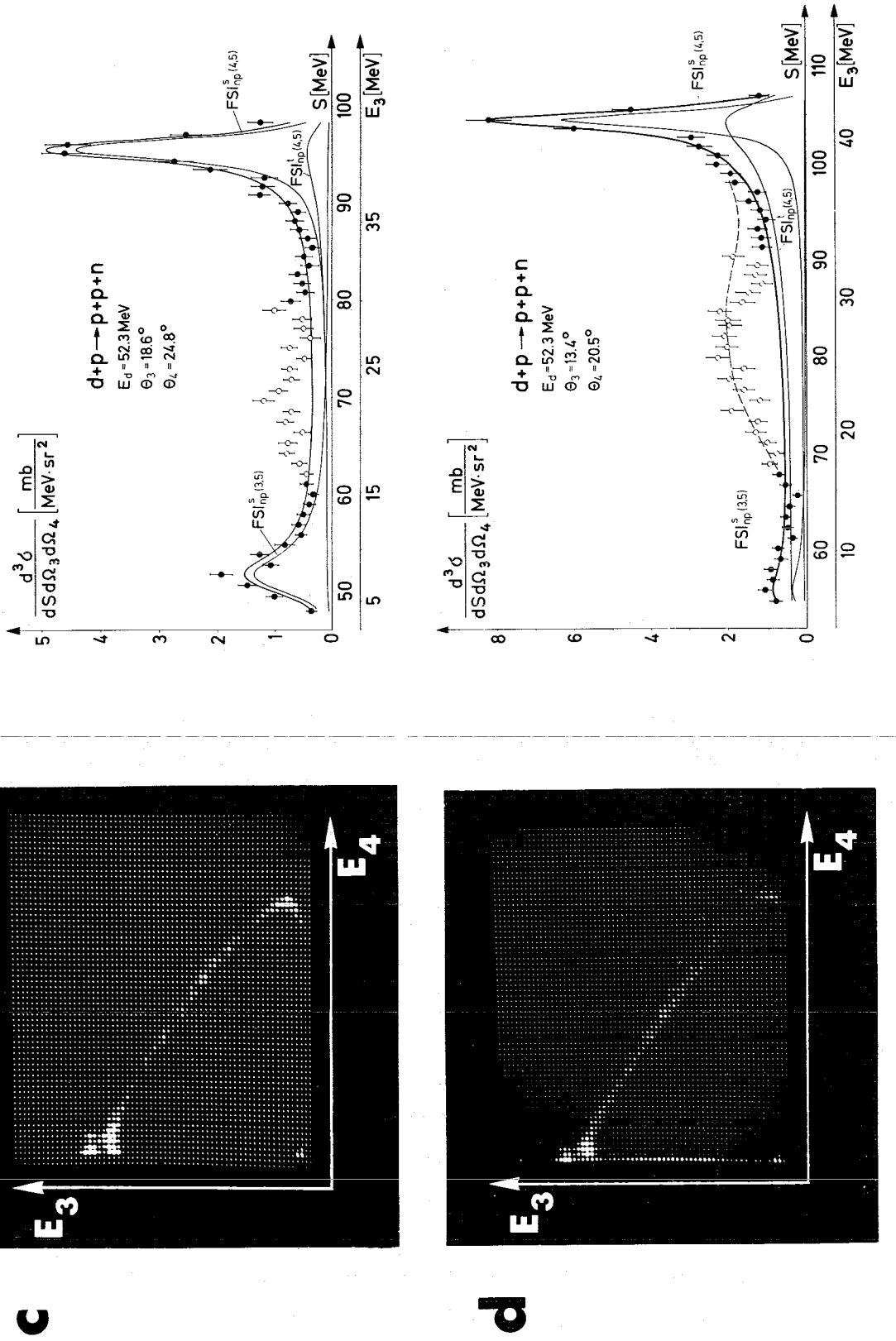

c d

Fig. 4c)

Experimental data for the set of angles θ_3=18.6° θ_4=24.8°
For denotation see Fig. 3

Fig. 4d)

Data taken at the angles θ_3=13.4 and θ_4=20.5°

Contrary to Fig. 2 the Fig. 4 b-d show examples where pairs of angles in the vicinity of the unique symmetrical position have been chosen. Although two FSI peaks can be seen E_{np} becomes zero only at one of the peaks.

Analysing these spectra one has to account for the FSI of both n-p pairs. The expression (5) for the three-particle cross-section has to be replaced by

$$\frac{d^3\sigma}{dS d\Omega_3 d\Omega_4} = \left[X^s_{np}(\theta_3) \cdot F^s_{np}(E_{45}) + X^t_{np}(\theta_3) F^t_{np}(E_{45}) + X^s_{np}(\theta_4) F^s_{np}(E_{35}) + X^t_{np}(\theta_4) \cdot F^t_{np}(E_{35})\right] \cdot \rho_S(E_3, E_4) \qquad (7)$$

Interferences between the (3,5) and (4,5) FSI amplitudes have been neglected.

The n-p pairs (3,5) and (4,5) are produced at different angles and five independent parameters had to be determined from each spectrum. These parameters are a^s, $X^s_{np}(\theta_3)$, $X^s_{np}(\theta_4)$, $X^t_{np}(\theta_3)$, $X^t_{np}(\theta_4)$. They were determined by least-square-fit calculations from the fraction of the data which is plotted with full dots. The results of the calculations are represented by the full curves in Fig. 4a-d. In the symmetrical situation (Fig. 4a) the experimental data are fitted excellently by the calculated curves. The FSI-ansatz used obviously seems to be adequate to reproduce the data in the whole kinematical region. Other reaction mechanisms are not interfering. At angles which are only approximately symmetrical the experimental data are not adequately reproduced. With decreasing angles one observes increasing disagreement with the FSI calculations (regions where the data are plotted by open circles). This disagreement results from an increasing contribution of the quasielastic scattering at forward angles.

For an interpretation of the data shown in Fig. 4 a-d a more detailed theoretical treatment is required. According to Bethe and Gluckstern [15] and Gammel et al. [16] in first Born approximation six graphs must be considered for the p-d reaction.

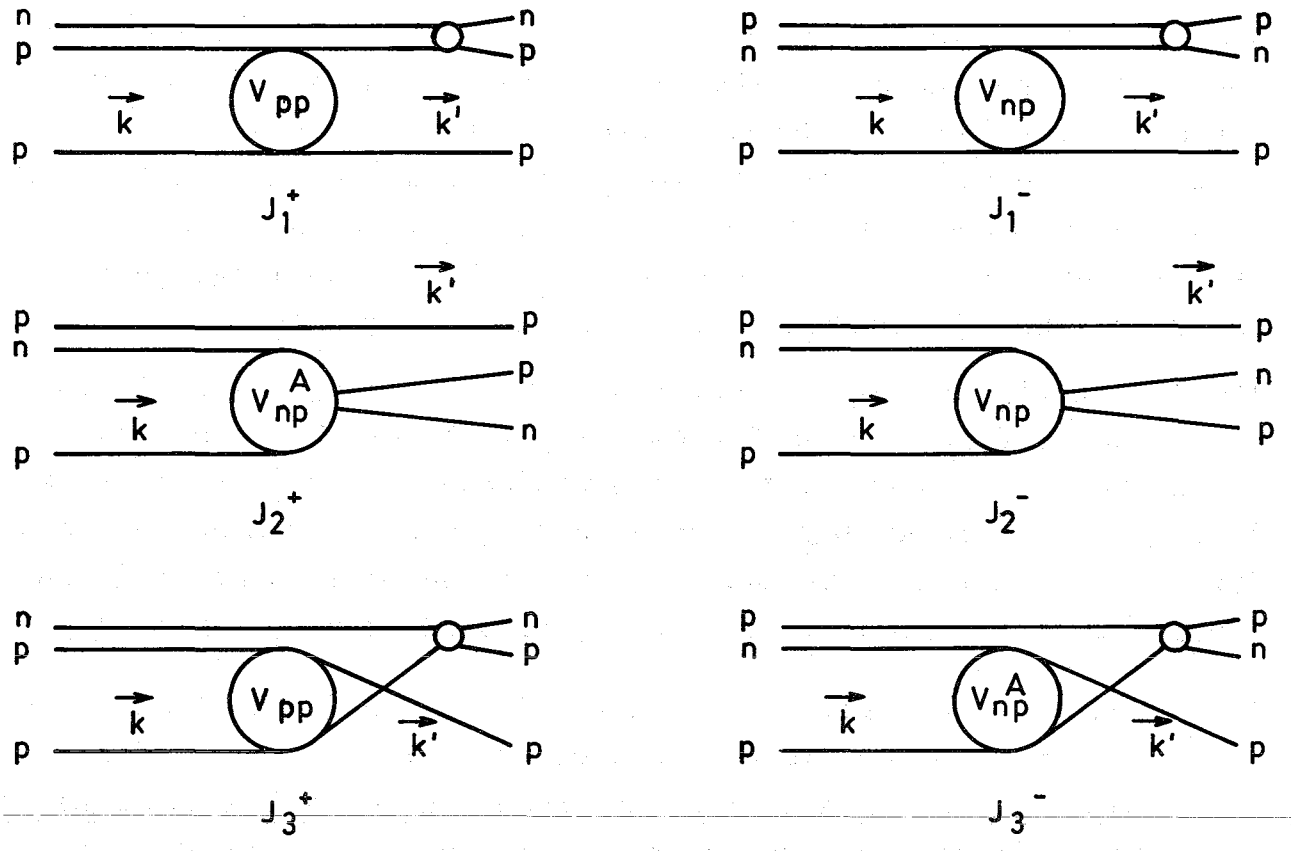

Fig. 5 a) The six basic graphes for the p-d reaction in first Born approximation. The first step is assumed to be a quasielastic proton-nucleon scattering. In the second step only n-p FSI is taken into account.

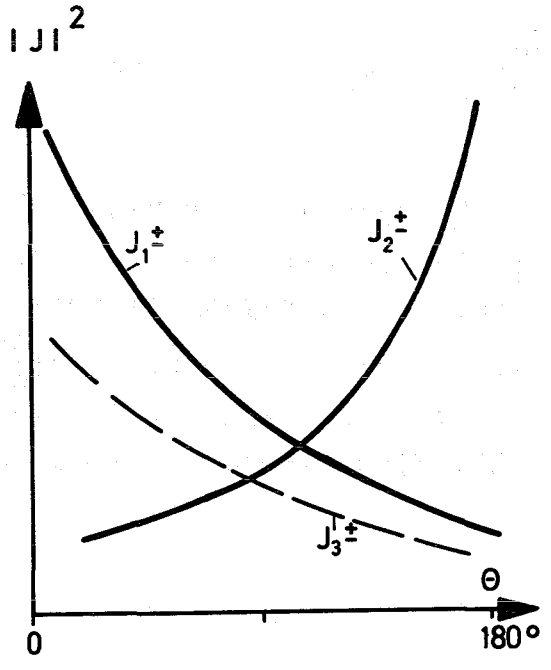

b) The contributions of the different graphs of Fig.5a are shown qualitatively as a function of the emission angle θ_d^* of the final state interacting n-p pair.

The graphs shown in Fig. 5a describe the first reaction step as a quasielastic scattering between the free proton and one of the nucleons in the deuteron. The second step accounts for the final state interaction. The graphs shown in Fig. 5a contain neutron-proton FSI only. This restriction is a good approximation for low relative neutron-proton energies E_{35} and E_{45}. In this case the relative energy of the two protons $E_{pp} = E_{34}$ is so large that contributions of a proton-proton FSI can be neglected.

The contributions from the different graphs to the cross-section are strongly dependent on the emission angle $\theta = \theta_d^*$ of the low energy neutron-proton pair. This dependence is shown qualitatively in Fig. 5b. At large angles the graphs $J_2^{\pm}$ are the dominating ones. Therefore an attempt was made to explain the data taken at large center-of-mass angles θ_d^* with the graphs $J_2^{\pm}$ only ($\theta_d^* > 140^\circ$).

The graph $J_2^{\pm}$ is a specific one in the sense that it is taken to be a disconnected graph. The FSI is already included in the first step and the graph $J_2^{\pm}$ describes the reaction mechanism in terms of a quasielastic neutron-proton scattering only. Consequently it is more suitable in this specific case to use for the quasielastic n-p scattering the impulse approximation [4b,5] than the first order Born approximation. In the impulse approximation the cross-section is given by

$$\frac{d^3\sigma}{d\Omega_3 d\Omega_4 dS} = \text{const} \quad |\psi_d(k_3^i)|^2 \cdot \left(\frac{d\sigma}{d\Omega}\right)_{np} \cdot \rho_S \qquad (8)$$

where k_3^i is the internal momentum of the spectator proton (particle 3) in the deuteron, $|\psi_d|^2$ is the Fourier transform of the deuteron wave function and $\left(\frac{d\sigma}{d\Omega}\right)_{np}$ is the off-energy-shell cross-section for n-p scattering (particles 4 and 5). Conveniently $\left(\frac{d\sigma}{d\Omega}\right)_{np}$ is replaced by the on-shell neutron-proton cross-section taken at the relative energy $E_{np} = E_{45}$ of the final state interacting n-p pair.

The largest angle θ_d^* at which the reaction p+d → p+p+n has been investigated is 152°. The corresponding experimental data are shown in Fig. 4d. These data are compared with a calculation based on ansatz (8). The result of the calculation is represented by the dashed curve of Fig. 4d. The ansatz fits the data nearly along the whole kinematical curve, while the Watson calculation (full curve) is only able to reproduce the FSI peak. The two factors of formula (8) show quite a different energy dependence. The factor $|\psi_d|^2$ has its maximum at a minimum value of k_3^i. The minimum corresponds in Fig. 4d to S=80 MeV. The n-p cross-section $\left(\frac{d\sigma}{d\Omega}\right)_{np}$ has a maximum at E_{45}=0 corresponding to S=105 MeV in Fig. 4d. At low relative energies the spectator model is identical with the Watson model because the cross sections $\left(\frac{d\sigma}{d\Omega}\right)_{np}$ for neutron-proton singlet and triplet scattering are proportional to the enhancement factors $F^s_{np_2}$ and F^t_{np} in very good approximation and the factor $|\psi_d|^2$ varies only slowly with energy in the region of FSI.

Table 1 summarizes the results of the analysis for the different pairs of angles investigated. The extracted n-p singlet scattering length is given together with the cross-sections for the n-p singlet and triplet FSI at E_{np}=0. The angular distribution of the singlet and triplet cross section are shown in Fig. 7 and will be discussed in section 3.2.2.

Table 1 Numerical results of the analyses

θ_3/θ_4	θ_d^*	a^s [fermi]	$\sigma^s \left[\frac{mb}{MeV \cdot sr^2}\right]$ for E_{np}=0	$\sigma^t \frac{mb}{MeV \cdot sr^2}$ for E_{np}=0
13.4/20.5	152	$-21\ ^{+1}_{-2}$	7.3±0.7	2.0±0.3
18.6/24.8	141	-15.9±2	5.0±0.5	0.4±0.15
23.0/26.8	131.8	-20.2±1.5	5.4±0.5	0.15±0.04
23.0/26.8	123.8	-	8.1±1.0	0.5±0.1
27.7/27.7	121.8	-20.2±1.5	10.1±1.0	0.4±0.3
42.0/25.3	91.6	-23.2±0.6	9.6±1.0	1.66±0.15
44.5/24.25	86.2	-22.0±0.8	8.9±0.9	1.78±0.2
48.3/22.4	78.0	-22.2±0.8	7.3±0.7	2.60±0.25
52.2/20.5	70.0	$-24.5^{+1.5}_{-2.5}$	7.4±0.7	2.87±0.3
56.0/18.25	60.8	$-27\ ^{+2}_{-3}$	8.75±0.9	3.44±0.35
58.5/16.7	55.0	-19.1±2	7.0±0.7	4.04±0.4

The scattering lengths obtained are plotted versus the production angle θ_d^* in Fig. 6. The value of the free n-p scattering length a_{np}^s = - 23.68 fm is indicated by a dashed line. Preliminary results have been already reported at the Birmingham conference |6| *. The best agreement with the free scattering length is achieved at production angles θ_d^* between 70° and 90°. As was already shown in the discussion of Fig. 3 one expects the most reliable determination of a_{np}^s in such an angular region, where the FSI is almost undisturbed by other contributing reaction mechanisms.

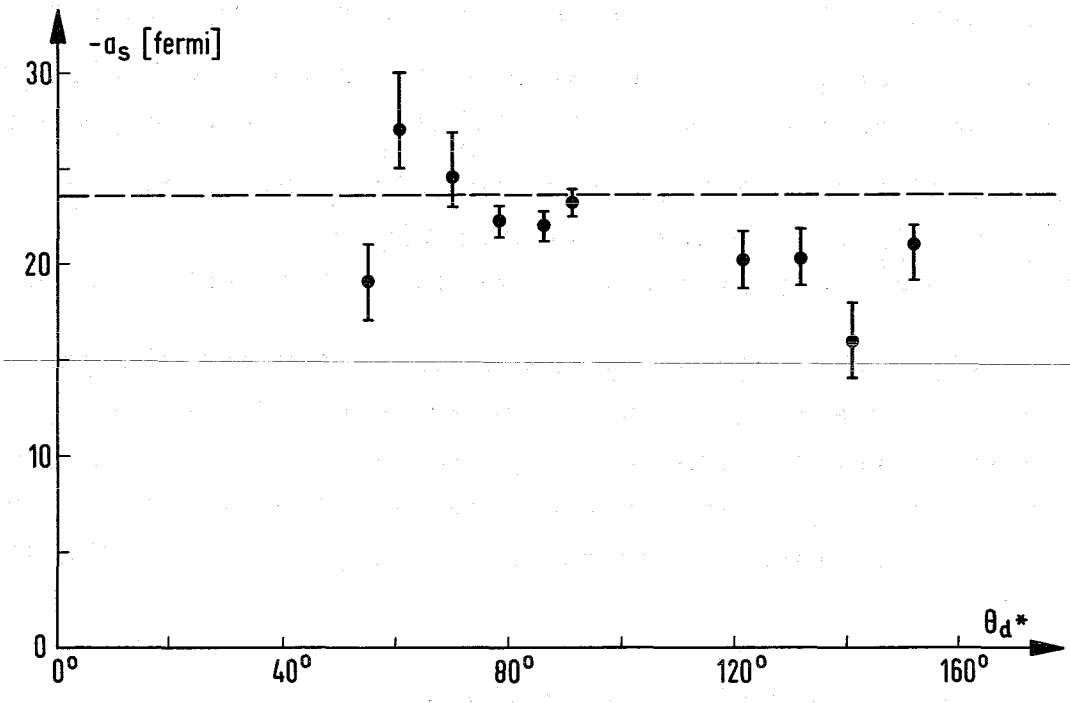

Fig. 6
The singlet n-p scattering length a^s obtained by analysing the three-particle cross-section at different angles θ_d^*. The dashed line indicates the scattering length known from free n-p scattering (a^s=-23.68 fm).

---

* Unlike to the present report the angle θ_{p3} has been used as abscissa and finite experimental resolutions had not jet been included.

To check the consistency of the analysis the least-square-fit calculations have been repeated with different numbers of experimental points. The error flags shown in Fig. 6 do not represent the statistical errors only but contain also the variation due to the different number of points included. For production angles at about 80° the analysis is largely independent on the chosen number of points. The resulting error of a^s is small as shown in Fig. 6. The mean value obtained for the scattering length from the three measurements at $\theta_d^* = 78.0^{\circ}$, 86.2°, 91.6° is $a^s_{np}=(-22.7\pm0.5)$ fm. A good agreement with the value known from the free n-p scattering is achieved.

In general one has to be very careful with the extraction of the scattering length by using the simple Watson model. Accurate values will only be obtained at conditions where no other reaction mechanisms interfere with the FSI of one neutron-proton pair. At the c.m. energy of our experiments the purest FSI is observed near $\theta_d^* = 80^{\circ}$, while at smaller or larger angles θ_d^* one finds a considerable poorer agreement with the predictions of the Watson theory. This result is of specific interest in using the same procedure to determine the neutron-neutron scattering length [4b] from the reaction n+d → n+n+p.

3.2.2 Discussion of the angular distribution

Fig. 7 shows the laboratory cross-section at relative energy $E_{np}=0$ for the production of n-p pairs in the singlet and triplet states (data from table 1). The cross-sections are plotted in a linear scale as a function of the production angle θ_d^* of the low energy n-p subsystem.* The angular distributions exhibit remarkable different shapes. The triplet cross-section decreases monotonously to a minimum at $\theta_d^*=130^{\circ}$ subsequently it increases at the backward angles. Contrary the singlet contribution has a maximum at $\theta_d^*\approx110^{\circ}$ which is followed by a steep decrease and a minimum at 140°.

* An angular distribution for the three-particle cross-section has been obtained in a less elaborate analysis where the singlet and triplet state contributions have not been separated [17].

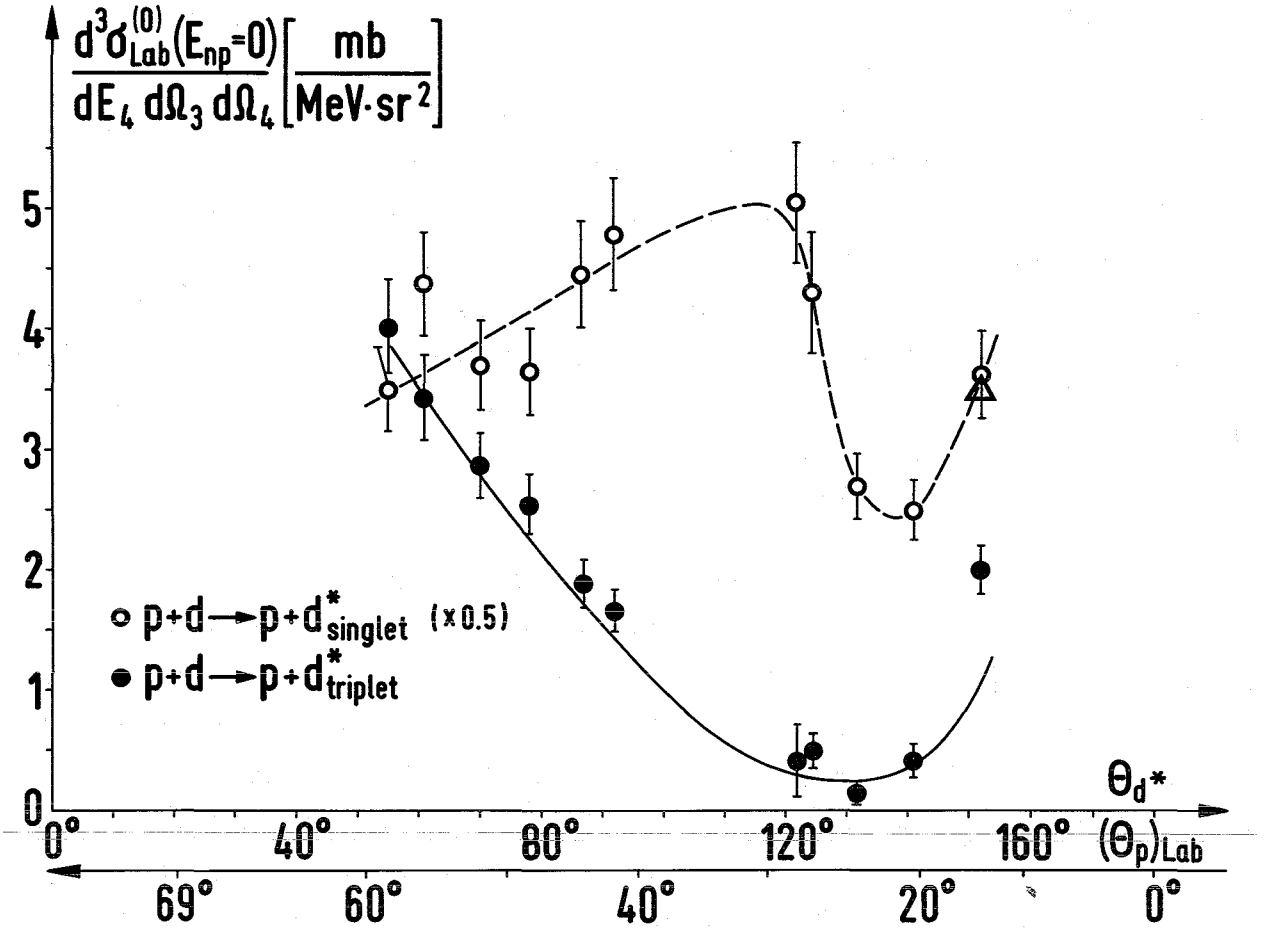

Fig. 7

The angular distribution of the three-particle cross-section for the production of final state interacting singlet and triplet n-p pairs with relative energy $E_{np}=0$. As abscissa the angle θ_d^* as well as the lab. angle of the "free" proton θ_p^{lab} are chosen. The solid curve is the result of a calculation which connects the three-particle cross-section quantitatively with the cross section of elastic p-d scattering. The triangle denotes the prediction for the singlet cross-section at a backward angle.

Comparing the angular distribution of the triplet cross-section with the cross-section of elastic deuteron-proton scattering [5] one observes a remarkable similarity of the two distributions. The question arises whether the triplet angular distribution of the three-particle reaction can be understood with the knowledge of the elastic proton-deuteron scattering.

The quantitative relation to be deduced has to connect reactions

$$p+d \rightarrow p+d \qquad (9a)$$

$$p+d \rightarrow p+d^{*}_{triplet} \rightarrow p+p+n \qquad (9b)$$

The main difference between these two reactions is that the neutron-proton system is produced in a bound (Q = 0 MeV) and an unbound (Q = - 2.224 MeV) state respectively whereas the spin states of the bound deuteron and the triplet d^{*} are identical.

The relation required has to connect the two-particle cross-section $\left(\frac{d\sigma}{d\Omega}\right)_{elastic}$ of reaction (9a) and the three-particle cross-section $\frac{d^3\sigma}{dE_4 d\Omega_3 d\Omega_4}$ of reaction (9b). Consequently the two transition matrix elements have to be discussed. Taking into account the particle spins and the antisymmetrization of the wave functions the matrix element for the elastic p-d scattering can be written in the Born approximation in the following form

$$T_{fi}^{el} = (\psi_d \cdot e^{i\vec{k}''\vec{r}} \cdot \chi_f, \{1-PQ\} \cdot \{V_{pp}+V_{pn}\} \psi_d \cdot e^{i\vec{k}\vec{r}} \cdot \chi_i), \qquad (10)$$

The matrix element for the three-particle reaction (9b) leading to the neutron-proton triplet FSI is given by

$$T_{fi}^{tripl} = (\psi_\kappa \cdot e^{i\vec{k}'\vec{r}} \cdot \chi_f, \{1-PQ\} \cdot \{V_{pp}+V_{pn}\} \psi_d \cdot e^{i\vec{k}\vec{r}} \cdot \chi_i) \qquad (11)$$

ψ_d and ψ_κ are the wave functions of the deuteron and of the n-p subsystem in the triplet state with relative momentum κ. The relative energy of the n-p system is given by $E_{np} = \frac{\hbar^2\kappa^2}{M} \cdot (V_{pp}+V_{np})$ is the interaction potential between the incident deuteron and the target proton. $\vec{k}$ is the momentum of the proton in the entrance channel whereas $\vec{k}'$ and $\vec{k}''$ denote the momenta of the "free" proton in the inelastic and elastic exit channel respectively (see Fig.5a).

χ_i and χ_f are the spinors of the initial and final state. The operators P and Q exchange the space and spin coordinates of the two protons.

Comparing the two matrix elements there is firstly a slight difference between the values $\vec{k}'$ and $\vec{k}''$ which is caused by the binding energy of 2.224 MeV of the deuteron. At our energy this off-energy-shell effect can be neglected and at identical production angles $\theta_d = \theta_d^*$ the wave vektor $\vec{k}'$ is taken to be equal to $\vec{k}''$. Secondly there is a difference between the wave function of the deuteron and the wave function of the n-p pair in the FSI triplet state. The radial parts $u = \text{const} \cdot r \cdot \psi(r)$ of the wave functions were calculated for the deuteron and for a free n-p pair with E_{np}=0 keV. A square well potential with parameters which reproduce the neutron-proton scattering length and the effective range [18] was used. Fig. 8 shows the two wave functions normalized to u(r)=1 at their maximum value and the potential parameters.

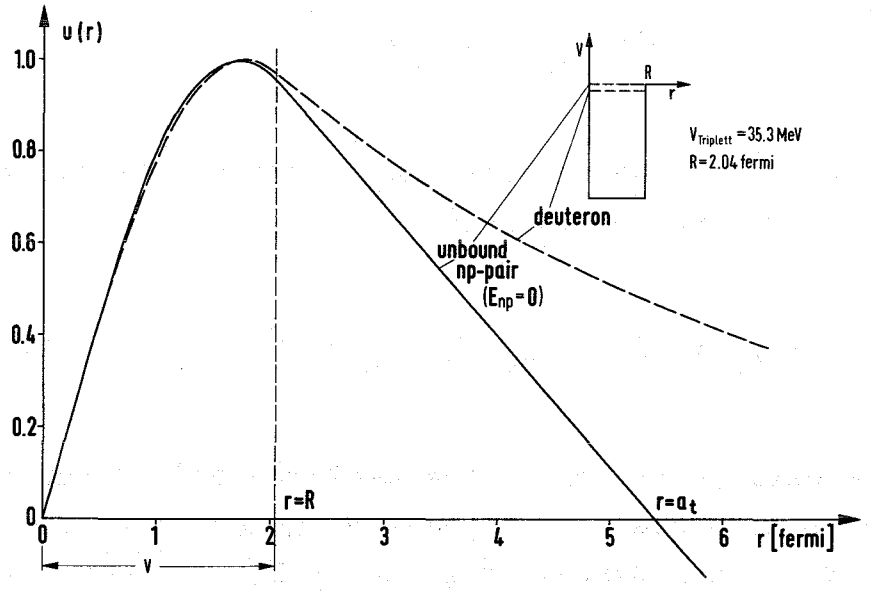

Fig. 8

Radial part of the deuteron wave function and the wave function of the unbound n-p pair in the triplet state at a relative energy E_{np}=0. The parameters for the square well potential used are given.

Within the range of the potential the two wave functions have nearly the same r-dependence. The differences are small because the free np-pair is taken to be produced with a relative energy $E_{np}=0$ and the deuteron binding energy is small compared with the potential depth $V = 35.3$ MeV . Therefore inside the potential well the shapes of the two wave functions are regarded to be identical.

Outside the range of the potential the two wave functions are very different. By discussion of all the graphs given in Fig. 5a it has been shown in Ref. [19] that the integrals over the internal coordinates of the deuteron and of the np-pair are only slightly affected by the shape of the wave functions outside the range of the np-potential provided the c.m. energy is large compared with the binding energy of the deuteron. Therefore contributions from outside the potential range can be neglected. With these assumptions the ratio of the matrix elements is given by

$$\frac{\left|T_{fi}^{tripl}\right|^2}{\left|T_{fi}^{el}\right|^2} = \left|\frac{\psi_\kappa(r=o)}{\psi_d(r=o)}\right|^2 \equiv \Phi\,(E_{np}) \qquad (12)$$

Where $\psi_\kappa(r=o)$ and $\psi_d(r=o)$ denote the values of the wave functions at the origin. In a good approximation $\Phi(E_{np})$ is proportional to the Watson enhancement factor F_{np}^t as defined by equation (4).

The square of the ratio of the wave functions $\psi_\kappa(r=o)$ and $\psi_d(r=o)$ was evaluated to be $\Phi\,(E_{np}=0) = 5.45\cdot10^{-37}\,cm^3$ at zero relative energy. This value was obtained by using the Hulthen wave function [16] for the deuteron and the continuum wave function for the np-pair as given by Gammel et al. [16]. The three-particle cross-section is given by

$$\frac{d^3\sigma_{tripl.}}{dE_4 d\Omega_3 d\Omega_4} = \frac{\rho_3}{\rho_2}\,\Phi\,(E_{np})\,\left(\frac{d\sigma}{d\Omega}\right)_{elastic} \qquad (13)$$

where ρ_2 and ρ_3 are the phase space factors for the reactions (9a) and (9b). The full curve of Fig. 7 was calculated using the data of the elastic proton-deuteron scattering at $E_d=51.5$ MeV [5] and

equation (13) at E_{np}=0 keV. A very good agreement between the experimental data and the calculated curve is obersved. The absolute magnitude as well as the angular dependence are surprisingly well reproduced.

Discussing the $J_2^{\pm}$ type of the graphs only Gammel and Frank have derived a relation between the three-particle and the two particle reaction cross-sections [16]. These authors conclude that the triplet and the singlet angular distribution should have the same shape. This prediction is in contradiction to our experimental results. In a more sophisticated discussion all the three types of graphs have to be considered as is shown in [19].

The successfull application of relation (13) proves that this formula can be regarded to be a widely generalized form of the Watson FSI formula. The absolute value of the three-particle cross-section can be evaluated from formula (13) as a function of the relative energy E_{np}, the center-of-mass energy and the production angle of the np-pair. In general the singlet neutron-proton FSI cannot be predicted from the elastic proton-deuteron scattering. Due to the spin dependence of the nuclear forces the singlet state is not comparable to the n-p triplet bound state (deuteron) and a bound singlet state of the neutron-proton system does not exist. The n-p singlet FSI and the elastic p-d scattering may be simply related at backward angles ($\theta_d^* > 140^\circ$) only. The contributions of the graphs $J_2^{\pm}$ dominate at these backward angles (see Fig. 5b). A ratio of the cross sections of n-p singlet and n-p triplet FSI can be predicted by using the relation for quasi-elastic n-p scattering (8). For zero relative energy one obtains

$$\frac{d^3\sigma_{\text{singlet}}}{dE_4 d\Omega_3 d\Omega_4} \Big/ \frac{d^3\sigma_{\text{triplet}}}{dE_4 d\Omega_3 d\Omega_4} = \frac{1}{3} \left(\frac{a^s}{a^t}\right)^2 \qquad (14)$$

a^s and a^t are the scattering lengths for np-singlet and triplet scattering. The three-particle cross-section of np-singlet-FSI was calculated for $\theta_d^* = 152^\circ$ and E_{np}=0 by use of the expressions (13) and (14)

$$\frac{d^3\sigma_{singlet}}{dE_4 d\Omega_3 d\Omega_4} = 7,1 \left[\frac{mb}{MeV \cdot sr^2}\right]$$

This value is shown in fig. 7 as a triangle. A very good agreement with the experimental result given in table 1 and fig. 7 is obtained.

A quite different point to be dicussed concerns the ratio of the number of elastically scattered deuterons to the total number of final state interacting np-pairs which are produced at a fixed angle θ_d^* and at the same conditions in the entrance channel. To evaluate the total number of neutron-proton pairs one has to integrate over the internal angular and momentum coordinates of the neutron-proton subsystem. Carriing out this integration

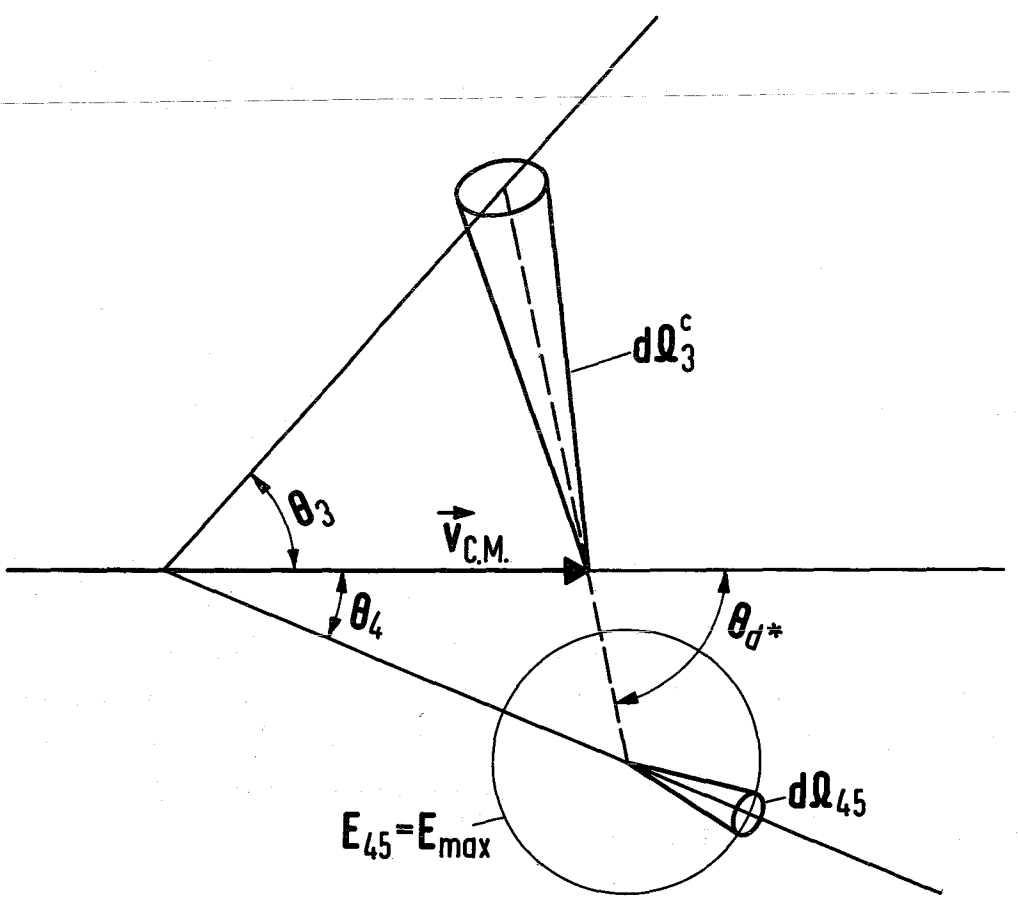

Fig. 9
Definition of the solid angles in the c.m.system of the n-p subsystem. The notation is used in equation (15).

separately for the singlet and triplet np-pairs one obtains the center-of-mass cross-section $\frac{d\sigma}{d\Omega_3^c}$ of the singlet and triplet FSI. These cross-sections are directly comparable with the elastic deuteron-proton cross section $\left(\frac{d\sigma}{d\Omega}\right)_{\text{elastic}}$

The laboratory three-particle cross-section was transformed into the recoil center-of-mass system of the np-pair see for notation Fig. 9 and e.g. Ref.10). Subsequently the integration was carried out over the solid angle Ω_{45} and the relative energy E_{45} of the neutron-proton subsystem. The d^*-system was assumed to be produced in a pure S-state corresponding to an isotropic np-angular distribution.

The integrated cross-section is

$$\frac{d\sigma}{d\Omega_3^c} = \left(\frac{d\sigma}{d\Omega_3^c}\right)_{\text{singlet}} + \left(\frac{d\sigma}{d\Omega_3^c}\right)_{\text{triplet}} = \int_{0}^{E_{max}} \int_{-\pi}^{\pi} \int_{0}^{2\pi} \frac{d^3\sigma}{dS\,d\Omega_3\,d\Omega_4} \frac{\partial(S,\Omega_3,\Omega_4)}{\partial(E_{45},\Omega_3^c,\Omega_{45})}\, dE_{45}\, d\Omega_{45} \tag{15a}$$

With equation (5) one obtains for the FSI of the n-p pair (4,5)

$$\frac{d\sigma}{d\Omega_3^c} = 4\pi \left[X_{np}^{s}(\theta_3) \int_{0}^{E_{max}} F_{np}^{s}(E_{45})\rho(E_{45})dE_{45} + X_{np}^{t}(\theta_3) \int_{0}^{E_{max}} F_{np}^{t}(E_{45})\rho(E_{45})dE_{45} \right] \tag{15b}$$

The integration can be carried out easily because the phase space factor $\rho(E_{45})$ in the center-of-mass system as well as the enhancement factor of the Watson ansatz are independent on the angular coordinates of the n-p subsystem (4,5). The values of X_{np}^{s}, X_{np}^{t} and a^s were already determined by the least-square-fit calculations discussed in section 3.2.1.

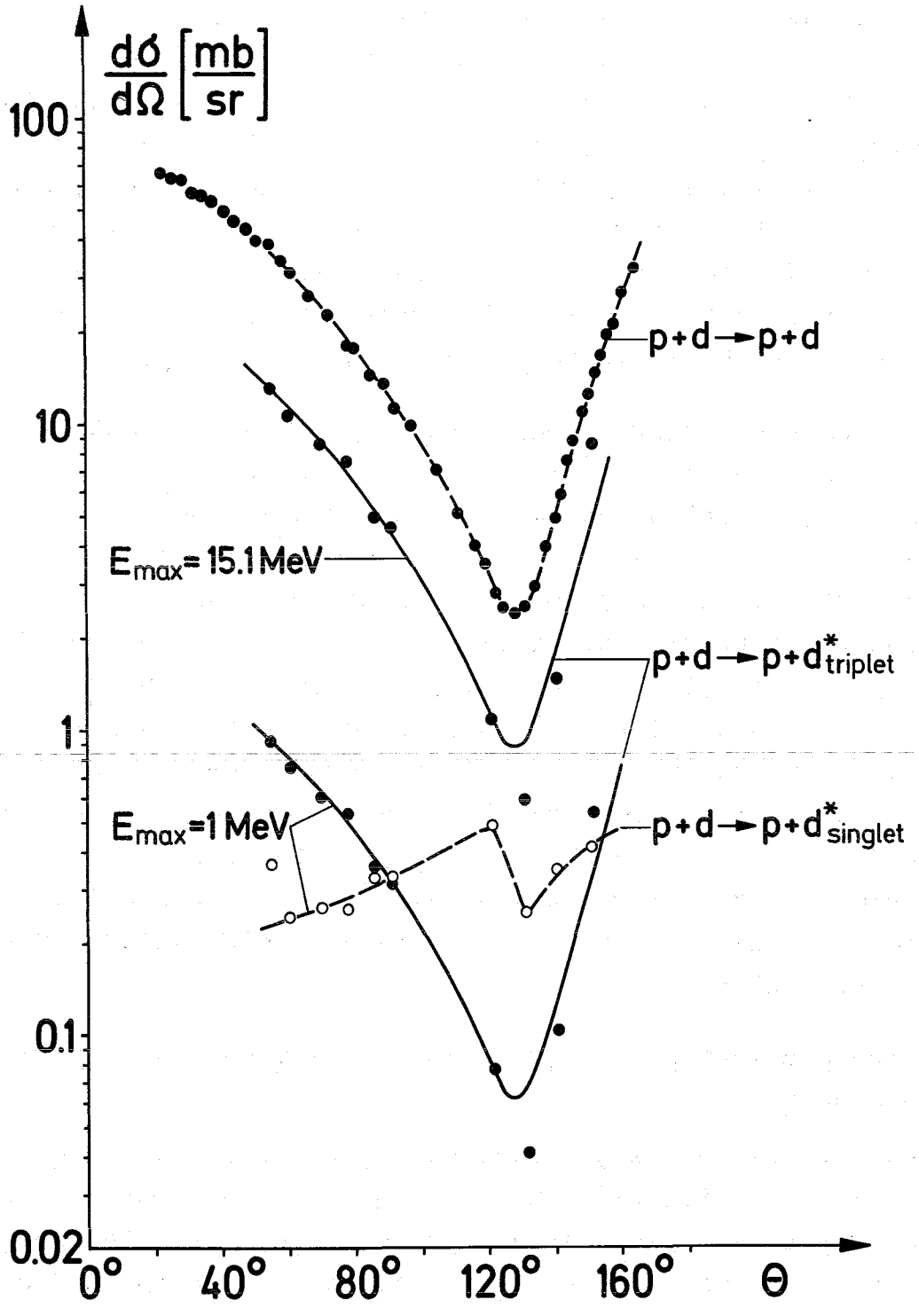

Fig. 10

The angular distribution of the cm cross-section for neutron-proton singlet and triplet FSI obtained by integration of the three-particle cross-section. For comparison the cross-section of elastic p-d scattering is also shown.

The total number of neutron-proton triplet and singlet FSI-pairs would be obtained by integrating up to the maximum energy available in the recoil center-of-mass system. In our experiment this energy is $E_{max}=E_{c.m.}=15.1$ MeV. An integration up to the maximum energy implies the validity of the enhancement factor $F_{np}(E_{np})$ at relative energies of up to 15.1 MeV. The Watson model, however, should surely not be extended to such high relative energies. Consequently the same integration has been carried out restricting only the limit to a lower value of $E_{max}= 1$ MeV.

Fig. 10 shows the center-of-mass cross-sections for neutron-proton singlet and triplet FSI integrated up to $E_{max}=1$ MeV. The result of an integration up to 15,1 MeV is only shown for the neutron-proton triplet state because the high energy region does not contribute appreciably to the singlet cross-section. For comparison the angular distribution of the elastic deuteron-proton scattering is also given in Fig. 10. The similarity between the angular distribution of the elastic deuteron-proton scattering and the neutron-proton triplet FSI is obvious. For ease of comparison two curves are shown which were obtained by multiplying the elastic cross-section by a properly chosen constant factor. The experimental data for the singlet neutron-proton FSI is connected by a dashed line and exhibits a significantly different angular distribution.

3.2.3 Proposed generalization of the results obtained to cluster phenomena

The three-particle cross-sections of the triplet neutron-proton FSI (Fig. 7) predicted with the knowledge of the elastic proton-deuteron scattering are in excellent agreement with the experimental results. For the reaction studied discussed in section 3.2.2 the wave functions of the bound deuteron and the triplet neutron-proton pair were known. By generalizing the validity of the method discussed above one might think of an extension of the procedure to such composite systems where information on the wave function is needed.

An example is ^{6}Li where one wants to determine the probability for the d-α-cluster configuration. Such a cluster probability might be measured by investigating the elastic scattering

$$\alpha + {}^6\mathrm{Li} \rightarrow \alpha + {}^6\mathrm{Li}$$

and the d-α final state interaction in the break-up reaction

$$\alpha + {}^6\mathrm{Li} \rightarrow \alpha + (\mathrm{d} + \alpha)$$

The energy necessary for the break-up of the ^{6}Li-nucleus into an α-particle and a deuteron is 1.5 MeV only. This binding energy is small compared to the interaction potential. Accordingly at $E_{\alpha d}$=0 the wave functions for the bound state and the final state interacting d-α pair should have nearly the same shape inside the interaction potential, if ^{6}Li can be considered to be a pure d-α cluster in the S-state.

Experimental data should answer the question whether the two angular distributions are similar and whether the absolute values of the break-up cross-sections can be predicted from the elastic α-^{6}Li scattering. Such an analysis should be able to reveal the d-α cluster probability. If a ^{3}He-triton cluster configuration should be dominating a different angular distribution would be observed. The procedure proposed might be advantageous compared to investigations by means of the quasielastic scattering because it accounts for all interactions between the projectile particle and the cluster constituents.

3.3. A test of the reliability of the two-step-reaction model

In this section another type of test for the Watson model will be discussed. Assuming a pure two-step process the production probabilities X^s_{np} and X^t_{np} defined in formula (5) should depend only on the production angle of the final state interacting n-p pair (θ_d*) and not on the internal angular coordinates in the n-p sub-system. In a coplanar two detector coincidence experiment the production angle θ_d* is in general a function of the relative energy $E_{np}=E_{45}$ and the angle θ_3 at which the "free" proton is detected. But for low relative energies the angle θ_d* is almost

independent on E_{np} and is therefore determined by θ_3 only. Consequently the production probabilities X^s_{np} and X^t_{np} are to be regarded as a function of θ_3 only (see equ. 5). To confirm these assumptions correlation experiments have been carried out. One detector was kept at a fixed position in the laboratory system while the internal angular coordinates in the np-subsystem under investigation were varied by moving the second detector. The situation is explained in Fig. 11.

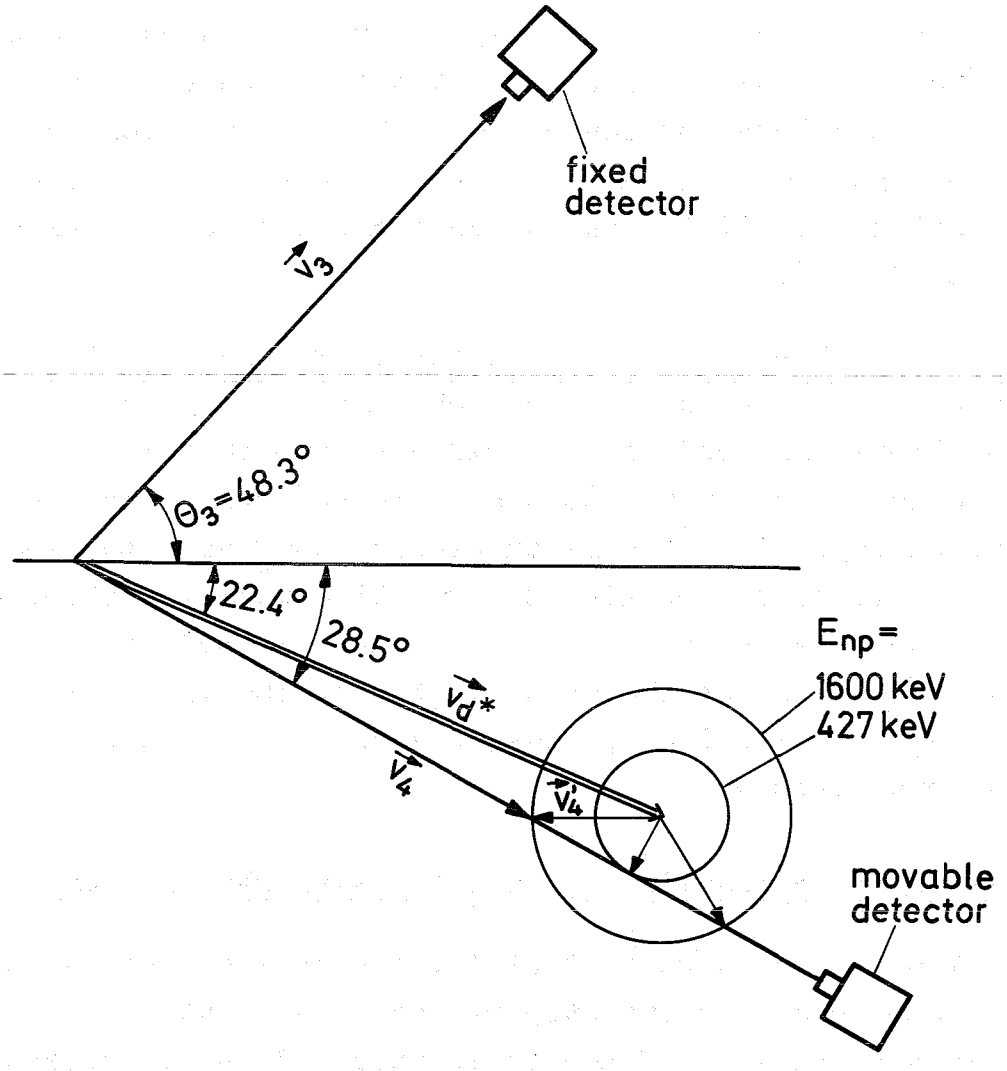

Fig. 11

The kinematical situation for the angular correlation experiments.

The fixed detector was positioned at θ_3=48.3°, the movable detector was placed at four angles of θ_4=20.0°, 22.4°, 26.5° and 28.5°. The velocity of the center-of-mass of the low energy neutron-proton pair is represented by the vector $\vec{v}_d$*. The relative energy E_{np} reaches down to the minimum possible value E_{np}=0 keV only if the detector is positioned in direction of $\vec{v}_d$* (θ_4=22,4°). At the other angles θ_4 the minimum relative energy is determined by the minimum relative velocity v_4' in the np-system. As is shown in Fig. 11 the value of the minimum relative energy is e.g. 427 keV at θ_4=28.5°. For the other angles θ_4=20.0° and 26.5° the minimum relative energies are 60 keV and 178 keV respectively.

Fig. 12 a-d show the coincidence spectra measured at four different angles θ_4. The spectra are given as a function of the arc length S defined by relation (1). The maximum of the reaction cross-section is always observed at the minimum of the relative energy E_{np}. The smaller the minimum possible relative energy the larger is the maximum value of the cross-section. Besides the well known FSI maximum the spectra taken at the angles θ_4=26.5° and 28.5° presented in Fig. 12c and 12d show an additional enhancement at low values of S. This enhancement is caused by a contribution of quasielastic proton-proton scattering which is expected in the region denoted by "n-spect" in Fig. 2a. In the following discussion this contribution of quasielastic scattering will be neglected.

The spectra of Fig. 12 were analysed in terms of ansatz (5). The equation (5) is explicitely based on the assumption that the production probabilities X_{np} depend on θ_3 only and that the enhancement factors F_{np} depend on the relative energy only. F_{np} does not contain any angular variables of the np-subsystem, this means that an isotropic distribution in the subsystem is assumed. The plausible arguement for this assumption comes from free low energy np-scattering where only the S-state contributes. Therefore one should be able to represent the whole information of the four spectra in Fig. 12a-d by determination of two free parameters only. These parameters are the two production probabilities $X_{np}^s(48.3°)$ and $X_{np}^t(48.3°)$. The angle θ_3=48.3° is convenient because the

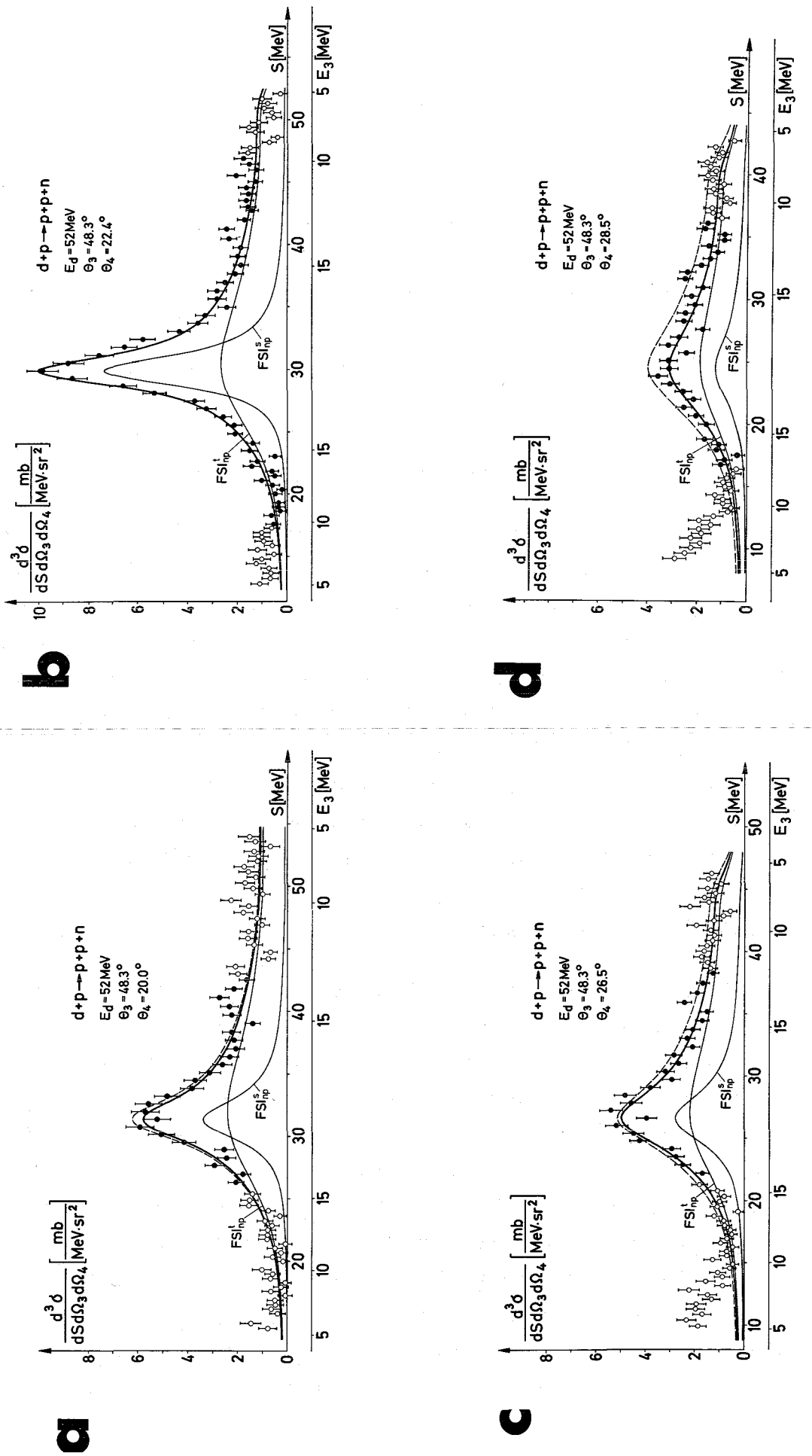

Fig. 12

Angular correlation spectra taken at a fixed angle θ_3=48.3°. Spectra a,b,c,d were obtained at θ_4=20.0°, 22.4°, 26.5° and 28.5° respectively.

scattering lengths determined in section 3.2.1 were found to be in good agreement with the free n-p scattering length at angles θ_3 between 42^o and 48^o. The analysis was carried out in the same manner as discussed in section 3.1 considering only the data denoted by full dots in Fig. 12 and using the scattering lengths and effective ranges of free n-p scattering.

Firstly the parameters X^s_{np} and X^t_{np} have been determined from the 22.4^o data of Fig. 12b only (analysis I). The cross-sections at the other angles θ_4 have been predicted with these parameters by using ansatz (5). The predictions are shown by dashed curves in Fig. 12a,c,d. The calculated curves and the measured spectra agree quite well. A slight discrepancy between the experimental data and the calculation is observed only in Fig. 12d.

Secondly the parameters X^s_{np} and X^t_{np} have been determined independently from each spectrum of Fig. 12 (analysis II). The results of the independent least-square-fit calculations are shown as full curves in Fig. 12a-d. Singlet, triplet and the sum of singlet and triplet contributions are presented separately. Fig. 13 shows the extracted parameters X^s_{np} and X^t_{np} in relative units as a function of the angle θ_4. Within the error flags the production probability for the singlet state X^s_{np} is independent on the angle θ_4. The production probability for the triplet state X^t_{np} however decreases slightly with increasing angle θ_4. The size of the error bars in Fig. 13 is partly due to errors in the relative monitoring of the different experiments. The ratio $QTS = X^t_{np} / X^s_{np}$ can be evaluated witz better accuracy because it contains only sthe statistical errors. As is shown in Fig. 14 the ratio QTS depends on θ_4 therefore the slight angular dependence of X^t is confirmed.

From these angular correlation measurements the following conclusions for the reliability of the two-step reaction model can be drawn: The experimental data can be described in a broad kinematical region with the two production probabilities X^s_{np} and X^t_{np} confirming the applicability of the model used. The singlet production probability X^s_{np} turns out to be independent on

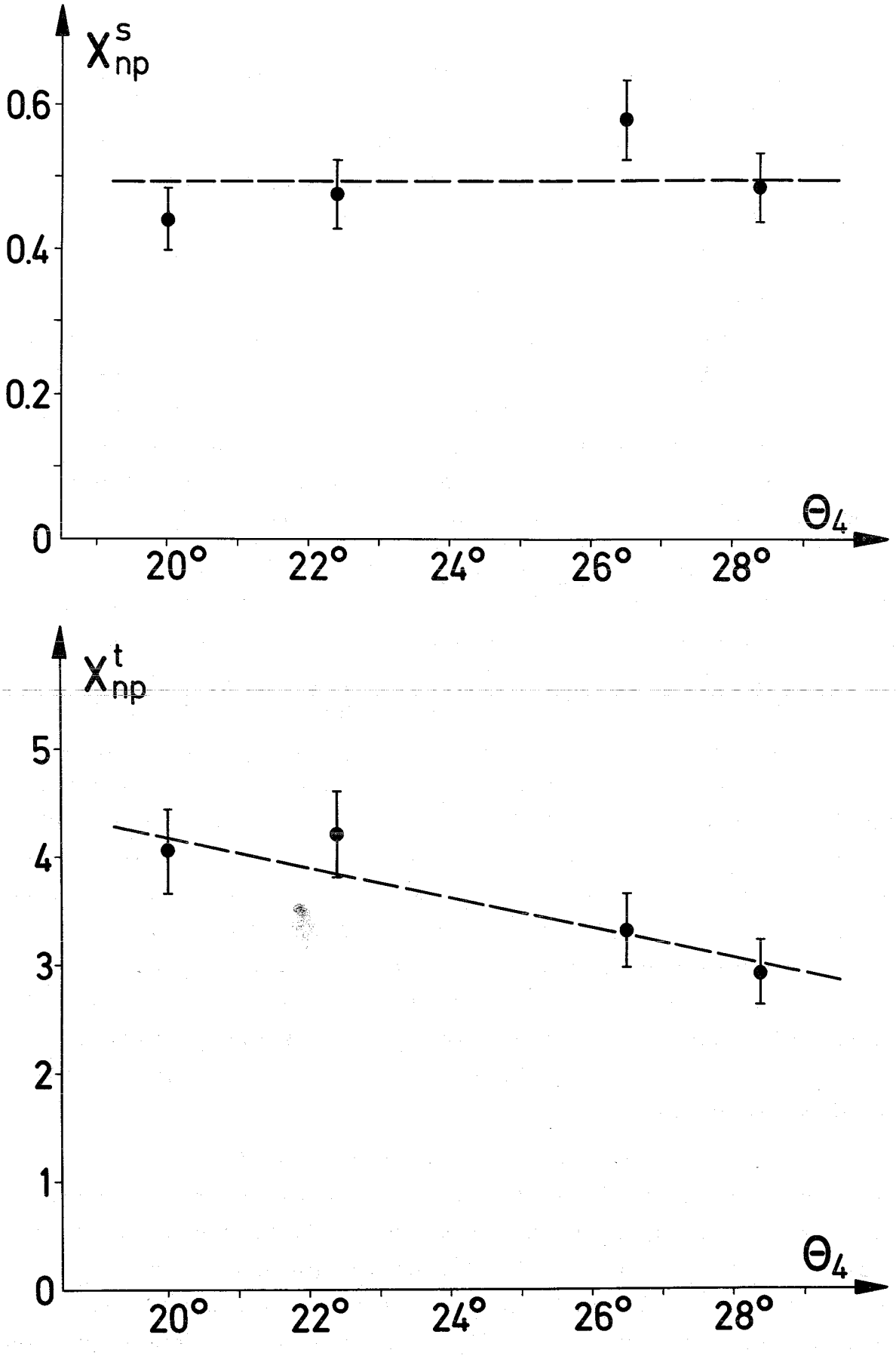

Fig. 13
The production probabilties X^s_{np} and X^t_{np} plotted as a function of the angle θ_4.

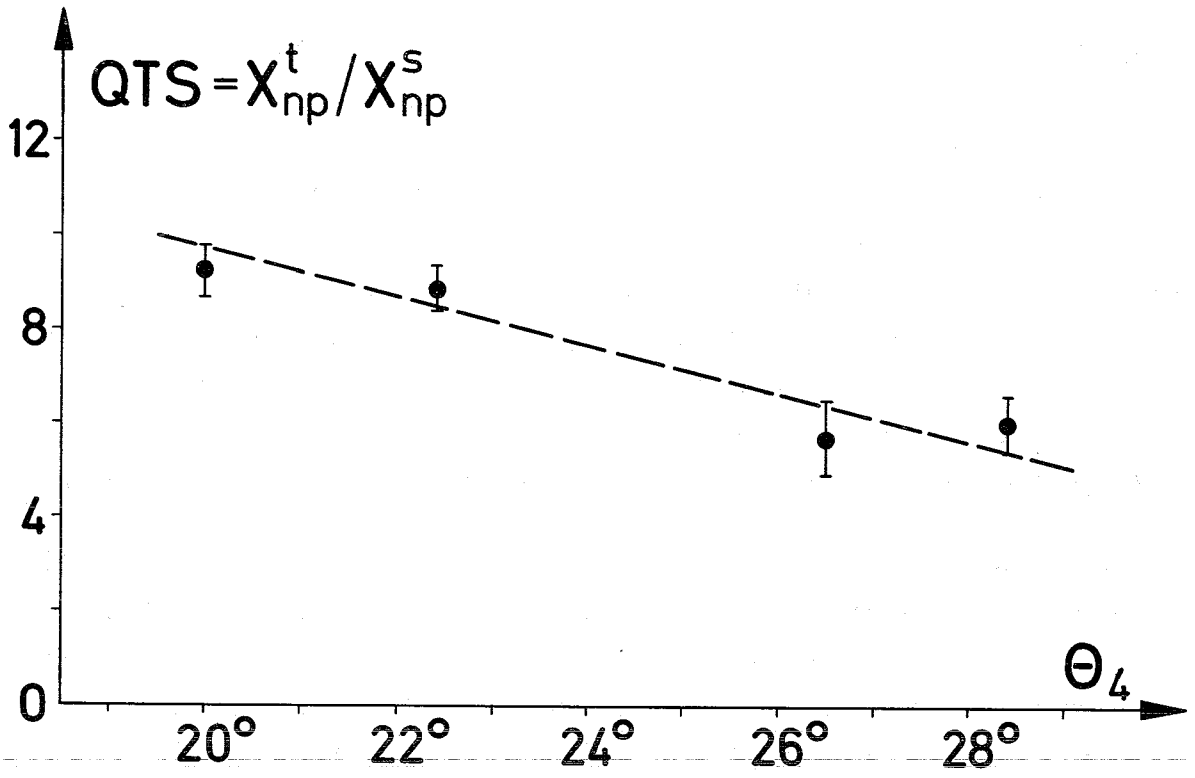

Fig. 14
The ratio of the triplet and singlet production probability plotted versus the angle θ_4.

the angle θ_4 whereas the slight variation of the triplet production probabilty X^t_{np} with θ_4 can be explained by the following considerations. Distortions from other reaction mechanisms have only a small influence on the neutron-proton singlet FSI while the triplet scattering is much more affected by other reaction mechanisms due to its considerably weaker energy dependence. Obviously the parameter X^t_{np} decreases at the angles where the contribution of the quasielastic proton-proton scattering increases (Fig. 12b-d at low values of S). A destructive interference between the quasielastic proton-proton scattering and the neutron-proton triplet FSI would explain such a decrease of the parameter X^t_{np}.

4. The proton-proton final state interaction in the reaction p+d → p+p+n

4.1 An experimental example and the methods of analysis

Encouraged by the results obtained from the analysis of the n-p FSI-data, also the proton-proton FSI was investigated systematically in the reaction p+d → p+p+n. The kinematical conditions were chosen to be the same as for the study of the n-p FSI. Instead of p-p coincidences n-p coincidences were observed by only changing the particle identification. From the experimental point of view this change in particle identification may be regarded as equivalent to "switching on" the Coulomb force.

Such systematic measurements are the essential part of the "comparison procedure" as discussed for instance by van Oers and Šlaus in reference [3b]. The basic idea of the comparison of p-p and n-p FSI in the same reaction and at identical experimental conditions is to get a more rigorous check on the reliability of special reaction models like the Watson-Migdal model.

But still another aspect should be stressed. The investigation of p-p FSI allows the effects of p-p interaction to be observed at very low relative energies where the experimental difficulties for free p-p scattering are nearly insurmountable. The reaction p+d → p+p+n is favoured because it is the simplest three-particle reaction leading to final state interacting p-p pairs.

The neutrons were detected with an angular resolution of $\Delta\theta_n = \pm 1.8^\circ$ by a plastic scintillator of 8 cm length and 7 cm in diameter. The neutron detection efficiency was determined by a Monte Carlo-calculation to be typically 18% at the maximum neutron energy where the p-p FSI is expected. The neutron energy is to be determined by a time-of-flight measurement. For this reason the experimental two-dimensial coincidence spectra are taken with the neutron time of flight and the energy of the coincident proton as coordinates.

An example of such an experimental map display is shown in Fig. 15b. The observed events populate the whole kinematical curve which is shown in the same scale in Fig. 15a. The data were analysed using the Watson-Migdal theory. A p-p scattering length of 7.5±0.5 fm was obtained [20].*

In the analysis of p-p final state interaction a modified Watson-Migdal enhancement factor F_{pp} has been used

$$F_{pp} = \frac{\left[\frac{1}{r_o} - \frac{1}{a_{pp}} + \frac{1}{2} r_o \kappa^2 + \frac{1}{R}\left(\ln \frac{r_o}{R} + 2\gamma - 1\right)\right]^2}{C^2(\eta)\,\kappa^2 + \frac{1}{C^2(\eta)}\left(-\frac{1}{a_{pp}} + \frac{1}{2} r_o \kappa^2 - \frac{h(\eta)}{R}\right)^2} \qquad (16)$$

In equation (16) r_o and a_{pp} denote the effective range and the p-p scattering length respectively. The value of R is given by $R = \hbar^2/M_p e^2 = 28.8\,\text{fm}$. M_p is the proton mass. γ is Eulers constant. κ is given by $\kappa = (M_p E_{pp}/\hbar^2)^{1/2}$ with E_{pp} the relative energy in the p-p center-of-mass system. The Coulomb penetration factor $C^2(\eta)$ is defined by $C^2(\eta) = 2\pi\eta/(e^{2\pi\eta}-1)$ with $\eta=(2\kappa R)^{-1}$. For low energies the factor $C^2(\eta)$ tends to zero, whereas it tends to 1 for large values of E_{pp} as well as for vanishing charge $e \to 0$.

The definition of $h(\eta)$ is given in [23]

$$h(\eta) = \text{Re}\left[\Gamma'(-i\eta)/\Gamma(-i\eta)\right] - \ln\eta = -\ln\eta - \gamma + \eta^2 \sum_{n=1}^{\infty} \frac{1}{n(n^2+\eta^2)} \qquad (17)$$

For small values of κ the κ dependence of the three-particle reaction matrix element can be factored out in form of an asymptotic S-wave function ψ_{pp} of the FSI proton pair.

$$\psi_{pp} = e^{-i\delta_o}\,(F_o \cos\delta_o + G_o \sin\delta_o)/\kappa r \qquad (18)$$

δ_o is the S-wave "nuclear phase shift". F_o and G_o are the S-wave regular and the irregular Coulomb wave functions which are used in the following expansions.

* Within the errors this value agrees with the free pp-scattering length $a_{pp} = -7.756 \pm 0.01$ fm [21].

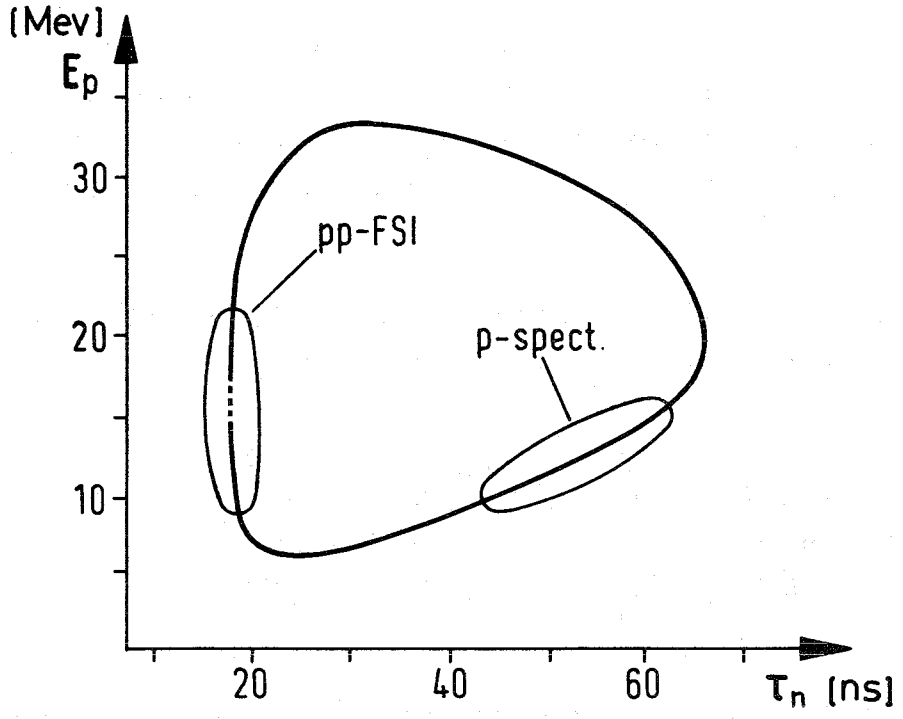

Fig. 15a)

The kinematically allowed curve in the E_p-τ_n plane. The region where p-p final-state interaction is expected is denoted by FSI. In quasielastic scattering a proton might be the spectator particle (p-spect.).

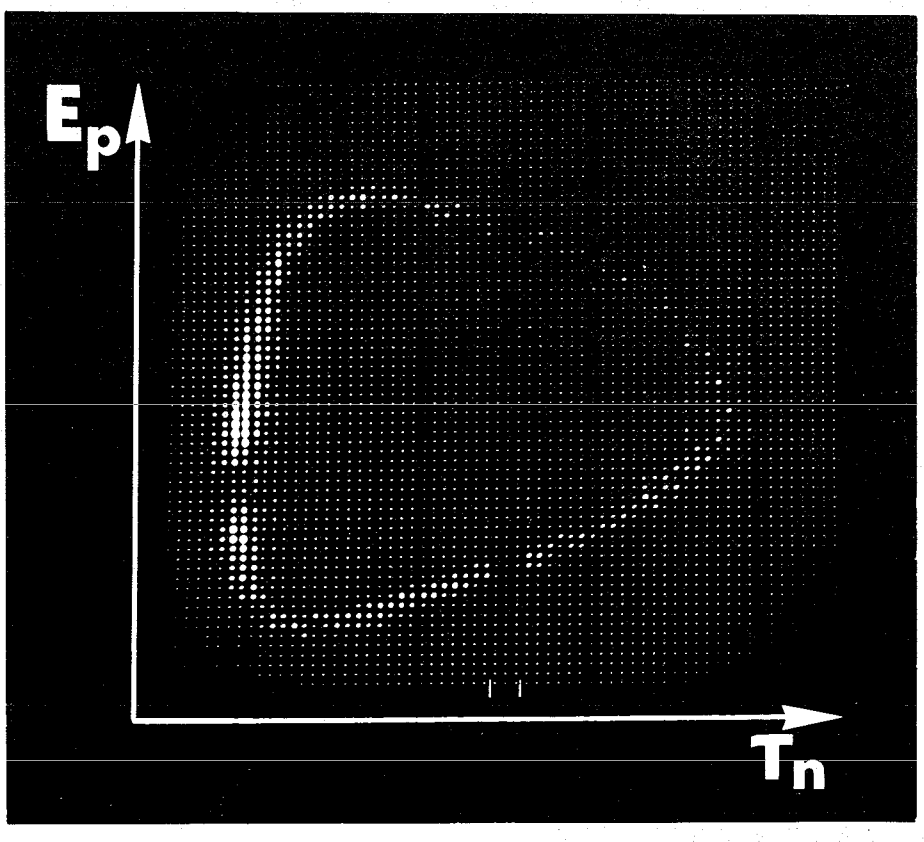

Fig. 15b)

The corresponding experimental data shown as a map display in an array of 64×64 channels.The detector angles were θ_n=420, θ_p=25.3°

$$F_o = C(\eta)\cdot\kappa r$$

$$G_o = \frac{1}{C(\eta)}\left[1+\frac{r}{R} < \ln\frac{r}{R} + h(\eta)+2\gamma-1 >\right] \qquad (19)$$

Substituting the well known shape independent p-p effective range expansion for the phase shift δ_o in equation (18) and inserting $r = r_o$ one obtains the enhancement factor $F_{pp} = |\psi_{pp}|^2$. Vacuum polarization in p-p scattering is neglected because this leads to very small corrections only [21]. It should be noticed that the denominator of the expression for F_{pp} given above is identical with the denominator of the original Migdal enhancement factor. The energy dependence of the nominator however influences considerably the value for a_{pp} extracted from p-p FSI data.

4.2 Measurement of the angular distribution in the p-p subsystem

Angular correlation experiments as discussed for neutron-proton FSI in sect. 3.3 provide an experimental method to establish the angular distribution in the subsystem of the final-state interacting particles if the two-step reaction mechanism holds. The applicability of the two-step reaction model was already confirmed for the n-p FSI where the angular distribution in the subsystem is known. Reasonably the two-step reaction model holds also in situations where the proton-proton final state interaction is observed in the same reaction and at identical kinematical conditions. Therefore one is able to investigate an anisotropy in the p-p subsystem angular distribution, which might be caused by a contribution of higher angular momenta in the Coulomb-interaction.

The angular distribution in the p-p subsystem of the two final state interacting protons was investigated by carrying out measurements with one fixed neutron and one movable proton detector. The general kinematical considerations are identical with those discussed for n-p FSI in section 3.3, only the particle detected at the angle θ_3 has to be the neutron and the d^* has to be

replaced by a p-p compound.

Two typical two-dimensional map displays for such an angular correlation measurement are shown in Fig. 16.

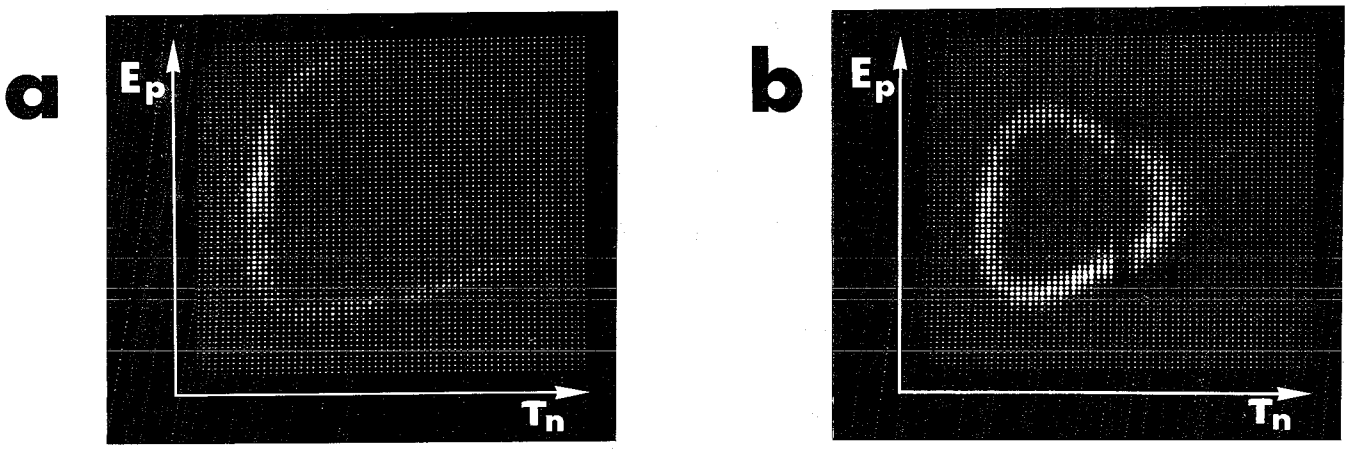

Fig. 16 Map displays θ_3=48.3°, θ_4=19.5°(a), θ_4=25.4°(b).

The data shown in Fig. 16 were taken at different angular positions of the proton detector θ_4 = 19.5° and θ_4 = 25.4°. Two additional spectra were observed at θ_4 = 22.4° and θ_4 = 28.3°. All these measurements were done with the neutron detector kept at a fixed angle of θ_3 = 48.3°.

The pronounced minimum to be seen in Fig. 15b does not appear in the other spectra because the relative energy does not reach down to zero. For the two spectra shown in Fig. 16 the minimum relative energy is E_{pp} = 85 keV (θ_4 = 19.5°) and E_{pp}=97 keV (θ_4 = 25.4°) respectively.

The distribution of final state events on the kinematical curve was projected onto the E_p-axis and divided by the phase space factor. The resulting squared three-particle matrixelement is shown in Fig. 17 as a function of E_{pp}.

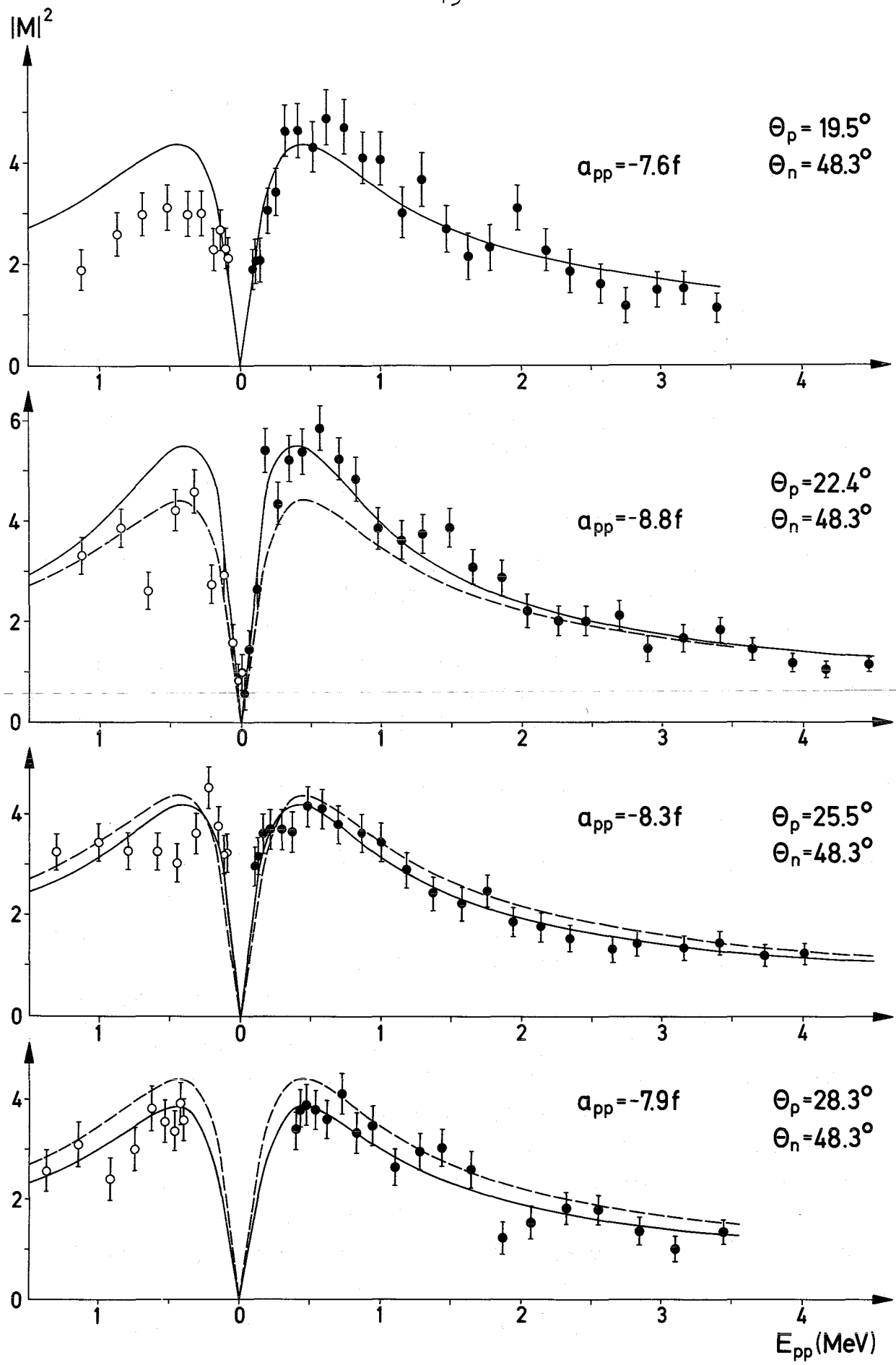

Fig. 17 Results of the angular correlation measurement for proton-proton FSI. $|M|^2$ was obtained, deviding the three-particle cross-section by the phase space factor ρ_3.

The data were analysed by using an ansatz of the form

$$|M|^2 = X_{pp} \cdot F_{pp}(E_{pp}) \qquad (20)$$

Two free parameters were used in the least square fit calculation namely the production probability X_{pp} and the scattering length a_{pp}. Only the points denoted in Fig. 17 by full dots were included into the analysis because at low proton energies (the corresponding points are denoted in Fig. 17 by circles) the spectator mechanism contributes more considerably. All the spectra exhibit an asymmetry between the points corresponding to the same relative energy E_{pp} but to different proton energies. As mentioned above (section 3.2) for the case of n-p FSI a reliable value for the scattering length a_{pp} will be obtained only, if there is no considerable contribution of other reaction mechansims than p-p FSI.

The experimental map display presented in Fig. 16a (θ_4=19.5°) shows the smallest spectator contribution and from the analysis a value of a_{pp} = 7.5 fm is obtained. Keeping in mind the spectator condition $\theta_3+\theta_4$ = 84° one expects an increasing contribution of the spectator effect with increasing angle θ_4. The validity of the assumption is demonstrated by the experimental map display in Fig. 16b. The spectrum observed at θ_4 = 25.4° shows a strong enhancement of events in the region which is denoted by p-spect in Fig. 15a.

The values of a_{pp} extracted from the data at different angles θ_4 vary between 7.4 fm and 8.8 fm. The full lines in Fig. 17 represent the results of the best least square fits. To compare the experimentally obtained results with an isotropic angular distribution in the p-p subsystem the 19.5° fit is plotted also in the three other spectra (dashed lines). Evidently the 19.5° fit shows at small relative energies only a moderate agreement with the other spectra indicating an anisotropy of the angular distribution in the p-p subsystem. At high relative energies

however the agreement between the four spectra is quite well. This good agreement at high relative energies is caused by a pure kinematical effect. The variation of the laboratory angle θ_4 corresponds to a variation of the p-p subsystem angle which is strongly dependent on the relative energy E_{pp}. At high energies E_{pp} this variation is considerably smaller than at low energies. The situation is illustrated in Fig. 11.

From the analysis discussed above two essential conclusions can be drawn for the proton-proton final state interaction.

1. It seems reasonable that the p-p FSI pair is formed in a ^1S_o-state predominantly.

2. On the other hand the angular correlation data cannot be completely reproduced by an analysis based on the simple form of the Watson-Migdal enhancement factor. A more realistic calculation is required including both the contribution of the spectator mechanism as well as the contribution of higher angular momenta in the Coulomb interaction. Such a calculation is in progress [22].

The authors want to express their gratitude to Prof. Dr. A. Citron, Prof. Dr. W. Heinz and Prof. Dr. H. Schopper for their encouragement and support.
We are indebted to Dr. H.J. Zeh for many valuable discussions concerning the theoretical interpretation of the experimental results. We would like to thank Dr. F.K. Schmidt, W. Gehrke and R. Schlüfter for their assistance in the experiment.
The good cooperation of Dr. G. Schatz and the members of the cyclotron staff is gratefully acknowledged.

References:

[1] a) L.D. Faddeev JETP 12, 1014 (1961)

b) C. Lovelace Phys.Rev. 135, B 1225 (1964)

c) A.C. Phillips Phys. Rev. 142, 984 (1966), Phys. Rev. 145, 733 (1966)

d) E.O. Alt, P. Grassberger, W. Sandhas, Nucl. Phys. B2, 167 (1967)

e) P. Grassberger, W. Sandhas, Nucl. Phys. B2, 181 (1967)

f) L.M. Delves, A.C. Philips, Rev.Mod. Phys. 41, 497 (1969)

[2] a) R. Aaron, R.D. Amado, Y.Y.Yam, Phys. Rev. 140, B 1291 (1965), Phys. Rev. 150, 857 (1966)

b) R.T. Cahill, I.H. Sloan, Proceedings of the Conf. on the Three Body Problem, p. 265, Birmingham 1969

[3] a) W.T.H. van Oers, Nucleon-nucleon scattering parameters from three-particle final state interactions, Preprint of the University of Winitoba, Winnipeg, Canada 1968

b) W.T.H. van Oers, I. Šlaus, Phys. Rev. 160, 853 (1967)

[4] a) I. Slaus, J.W. Verba, J.R. Richardson, R.F. Carlson, L.S. August, Phys. Letters 23, 358 (1966)

I. Slaus, Proc. of the Conf. on the Three Body Problem, p. 337, Birmingham 1969

b) B. Zeitnitz, R. Maschuw, P. Suhr, Phys.Lett. 28B, 420 (1969), DESY Report 70/7 (1970)

c) A.F. Kuckes, R. Wilson, P.F. Cooper, Ann.Phys. 15, 193 (1961)

d) B. Kühn, H. Kumpf, K. Möller, J. Mösner, Nucl.Phys. A 120, 285, (1968)

e) H. Jermemie, T. Grandy, Nucl.Phys. A 132, 571 (1969)

f) W.D. Simpson, W.R. Jackson, G.C.Phillips, Nucl.Phys. A 103, 97 (1967)

A. Niiler, C. Joseph, V. Valković et al. Phys.Rev. 182, 1083 (1969)

g) D.P. Boyd, P.F. Donovan, J.F. Mollenauer, The proton-neutron final state interaction, Preprint Rutgers State University 1968

h) J. Arvieux, J.L. Durand, A. Papineau, A. Tarrats, Proceedings of the Conf. on the Three Body Problem, Birmingham 1969

i) M. L'Huillier, N. Marty, M. Morlet, B. Tatischeff, A. Willis Proceedings on the Conf. on the Three Body Problem, p. 430, Birmingham 1969

j) W.J. Braithwaite, J.M. Cameron, D.W. Storm, D.J. Margaziotis, G. Paić, J.G. Rogers, J.W. Verba, J.C. Young, Proceedings of the Conf. on the Three Body Problem, p. 407, Birmingham 1969

[5] H. Brückmann, W. Kluge, L. Schänzler, Z.Physik 217, 350 (1968)

[6] H. Brückmann, W. Gehrke, W. Kluge, H. Matthäy, L. Schänzler, K. Wick, Proceedings of the Conf. on the Three Body Problem, p. 230, Birmingham 1969
Report of the Kernforschungszentrum Karlsruhe KFK 1012, 1969

[7] a) K.M. Watson, Phys. Rev. 88, 1163 (1952)
b) A.B. Migdal, Zh. Eksp. i Theor. Fiz. 28, 3 (1955)

[8] H. Brückmann, E.L. Haase, W. Kluge, L. Schänzler, Nucl.Instr. Meth. 67, 29 (1969)

[9] H. Brückmann, Report of the Kernforschungszentrum Karlsruhe KFK 912, 1968
H. Brückmann, P. Fluck, H. Matthäy, L. Schänzler, Report of the Kernforschungszentrum Karlsruhe KFK 897, 1968

[10] G.G. Ohlsen, Nucl. Instr. Meth. 37, 240 (1965)

[11] G.F. Chew, F.E. Low, Phys.Rev. 113, 1640 (1959)

[12] M.C. Goldberger, K.M. Watson, Collision Theory, Wiley & Sons, New York 1964, p. 479

[13] H. Brückmann, W. Gehrke, W. Kluge, H. Matthäy, L. Schänzler, K. Wick, Report of the Kernforschungszentrum Karlsruhe KFK 892, 1968

[14] H.P. Noyes, Phys.Rev. 130, 2025 (1963)

[15] R.L. Gluckstern, H.A. Bethe, Phys. Rev. 81, 761 (1951)

[16] a) R.M. Frank, J.L. Gammel, Phys.Rev. 93, 463 (1954)
b) R.S. Christian, J.L. Gammel, Phys.Rev. 91, 100 (1953)

[17] H. Brückmann, W. Gehrke, W. Kluge, H. Matthäy, L. Schänzler, K. Wick, Report of the Kernforschungszentrum Karlsruhe KFK 1130 (1970) (to be published in Z.Phys.)

[18] G.L. Squires, Progr. Nucl. Phys. 2, 89 (1953)

[19] K. Wick, Ph.D.Thesis, University of Karlsruhe 1970

[20] H. Brückmann, W. Kluge, H. Matthäy, L. Schänzler, K. Wick, Phys. Lett. 30b, 460 (1969)

[21] J. Birchall, C.O. Blyth, P.D. Dunscombe, S.Q.G. Mathaboally, J.S.C. Mc.Kee, B.L.Reece, M. Slobodrian, R.J. Slobodrian, Proceedings of the Conf. on the Three Body Problem, p. 423, Birmingham 1969
R.J. Slobodrian, Phys. Rev. Lett. 21, 438 (1968)

[22] H. Matthäy, Ph.D.Thesis, University of Karlsruhe 1970

[23] J.D. Jackson, J.M. Blatt, Revs.Mod.Phys. 22, 77 (1950)